



CERN-EP-2020-098
29 May 2020

Constraining the Chiral Magnetic Effect with charge-dependent azimuthal correlations in Pb–Pb collisions at $\sqrt{s_{NN}} = 2.76$ and 5.02 TeV

ALICE Collaboration*

Abstract

Systematic studies of charge-dependent two- and three-particle correlations in Pb–Pb collisions at $\sqrt{s_{NN}} = 2.76$ and 5.02 TeV used to probe the Chiral Magnetic Effect (CME) are presented. These measurements are performed for charged particles in the pseudorapidity (η) and transverse momentum (p_T) ranges $|\eta| < 0.8$ and $0.2 < p_T < 5$ GeV/ c . A significant charge-dependent signal that becomes more pronounced for peripheral collisions is reported for the CME-sensitive correlators $\gamma_{1,1} = \langle \cos(\varphi_\alpha + \varphi_\beta - 2\Psi_2) \rangle$ and $\gamma_{1,-3} = \langle \cos(\varphi_\alpha - 3\varphi_\beta + 2\Psi_2) \rangle$. The results are used to estimate the contribution of background effects, associated with local charge conservation coupled to anisotropic flow modulations, to measurements of the CME. A blast-wave parametrisation that incorporates local charge conservation tuned to reproduce the centrality dependent background effects is not able to fully describe the measured $\gamma_{1,1}$. Finally, the charge and centrality dependence of mixed-harmonics three-particle correlations, of the form $\gamma_{1,2} = \langle \cos(\varphi_\alpha + 2\varphi_\beta - 3\Psi_3) \rangle$, which are insensitive to the CME signal, verify again that background contributions dominate the measurement of $\gamma_{1,1}$.

© 2020 CERN for the benefit of the ALICE Collaboration.

Reproduction of this article or parts of it is allowed as specified in the CC-BY-4.0 license.

*See Appendix A for the list of collaboration members

1 Introduction

Heavy-ion collisions at ultra-relativistic energies are used to study the phase transition from a deconfined Quark–Gluon Plasma (QGP) state [1–3] to ordinary nuclear matter. The transition is expected to occur at high values of temperature and energy density, which is also supported by quantum chromodynamics (QCD) calculations on the lattice [4, 5]. The main aim of the heavy-ion program at the Large Hadron Collider (LHC) is to study the QGP properties, such as the equation of state, the speed of sound in the medium and the value of the ratio of shear viscosity to entropy density (η/s).

It was soon realised that heavy-ion collisions also allow for studies of novel QCD phenomena associated with parity (P) violation effects in strong interactions [6, 7]. These effects are catalysed by the presence of a strong magnetic field that develops in the early stages of heavy-ion collisions. This field is created by the motion of the charged nucleons of the incoming ions in a non-central collision, i.e. a collision with a large impact parameter, defined as the distance between the centers of the two colliding nuclei in the transverse plane. The magnitude of this field can reach values of 10^{18} Gauss [8], making it the strongest magnetic field created by any experiment on earth. The direction of the magnetic field is along the system’s angular momentum and perpendicular to the reaction plane. The latter is the plane defined by the impact parameter vector and the beam direction.

The potential to observe parity violation in the strong interaction using ultra-relativistic heavy-ion collisions has first been discussed in Refs. [9–11] and was further reviewed in Ref. [12, 13]. In QCD, this symmetry violation originates from the possibility that the QGP can carry net chirality [14–16], characterised by a non-zero value of the axial chemical potential μ_5 , i.e. reflecting the imbalance between left- and right-handed fermions in the system. Depending on the sign of μ_5 the QGP will have an excess of either left- ($\mu_5 < 0$) or right-handed ($\mu_5 > 0$) (anti-)quarks. In the presence of the strong magnetic field, the spins of (anti-)quarks tend to align along the direction of the field, creating a spin polarisation effect. This in turn leads to the development of a vector current along the direction of the magnetic field and the creation of an electric dipole moment of QCD matter. The experimental search for these effects has intensified lately, following the realisation that the subsequent creation of charged hadrons results in an experimentally accessible charge separation along the direction of this magnetic field, and perpendicular to the reaction plane. This phenomenon is called the Chiral Magnetic Effect (CME) and its existence was recently reported in semimetals like zirconium pentatelluride (ZrTe_5) [17].

The resulting charge separation can be identified by studying the P-odd sine terms in the Fourier decomposition of the particle azimuthal distribution [18] according to

$$\frac{dN}{d\varphi_\alpha} \sim 1 + 2 \sum_n [v_{n,\alpha} \cos(n\Delta\varphi_\alpha) + a_{n,\alpha} \sin(n\Delta\varphi_\alpha)], \quad (1)$$

where $\Delta\varphi_\alpha = \varphi_\alpha - \Psi_{\text{RP}}$ is the azimuthal angle φ_α of the particle of type α (either positively or negatively charged particles) relative to the reaction plane angle Ψ_{RP} . The coefficient $v_{n,\alpha}$ is the n -th order Fourier harmonic, averaged over all events, and characterises the anisotropies in momentum space. The reaction plane is not an experimental observable but can be approximated by the second-order symmetry plane, Ψ_2 , determined by the direction of the beam and the axis of the maximal particle density in the elliptic azimuthal anisotropy. This symmetry plane and more generally the plane angles of different order Ψ_n , estimated in each event, are introduced to account for the event-by-event fluctuations in the initial energy density of a heavy-ion collision [19–23]. In case of a smooth distribution of matter produced in the overlap zone, the angle Ψ_2 coincides with that of the reaction plane, i.e. $\Psi_2 = \Psi_{\text{RP}}$. The leading order P-odd coefficient $a_{1,\alpha}$ reflects the magnitude of the effects from local parity violation, while higher orders ($a_{n,\alpha}$ for $n > 1$) describe the specific shape in azimuth. However, the chiral imbalance that leads to the creation of the CME changes from event to event and the event average $\langle a_{1,\alpha} \rangle$ will be consistent with

zero. Consequently, the effect can be detected only by correlation studies.

In Ref. [24], it was suggested that a suitable way to probe the CME is via a two-particle correlation technique relative to the second-order symmetry plane of the form $\langle \cos(\varphi_\alpha + \varphi_\beta - 2\Psi_2) \rangle$, where the brackets indicate an average over all events. Here, α and β denote particles with the same or opposite electric charge. The advantage of using this expression is that it probes correlations between two leading order P-odd coefficients $a_{1,\alpha}$ and $a_{1,\beta}$ which do not trivially average to 0 over all events (see Section 3 for the discussion). In addition, the observable is constructed as the difference between correlations in- and out-of plane which is expected to significantly suppress parity-conserving background effects. In order to independently evaluate the contributions from correlations in- and out-of plane one measures at the same time a two-particle correlator of the form $\langle \cos(\varphi_\alpha - \varphi_\beta) \rangle$. Section 3 contains a detailed discussion about all these correlators.

Experimental results for charged particles in both Pb–Pb collisions at $\sqrt{s_{\text{NN}}} = 2.76$ TeV at the LHC [25] and in Au–Au collisions up to $\sqrt{s_{\text{NN}}} = 0.2$ TeV at the Relativistic Heavy-Ion Collider (RHIC) [26–30] are consistent with the expectation for a charge separation relative to the reaction plane due to the existence of parity violating effects. However, these measurements could be dominated by background effects whose sources have not been fully quantified yet. One of the first attempts to provide a quantitative estimate of the background in the measurement of the CME sensitive correlator (i.e. $\langle \cos(\varphi_\alpha + \varphi_\beta - 2\Psi_2) \rangle$) identified the sources as originating from local charge conservation coupled to the elliptic flow modulation quantified by v_2 [31, 32]. Therefore, the challenge is to define a way to constrain and quantify the background, while in parallel isolating the signal that comes from the CME.

A first step in this direction was taken by the ALICE Collaboration [33] using a method proposed and developed in Ref. [34]. This method, called Event Shape Engineering (ESE), utilises the fluctuations of the initial geometry and selects events with different initial system shapes, e.g. central Pb–Pb collisions with large initial anisotropy. This study set an upper limit of 26–33% at 95% confidence level for the CME signal contribution to the $\langle \cos(\varphi_\alpha + \varphi_\beta - 2\Psi_2) \rangle$ correlator in the 10–50% centrality interval. The CMS [35] and the STAR [36] collaborations studied charge-dependent correlations in p–Pb collisions at $\sqrt{s_{\text{NN}}} = 5.02$ TeV and in p–Au and d–Au collisions at $\sqrt{s_{\text{NN}}} = 0.2$ TeV, respectively. In these colliding systems, one expects the CME contribution to any charge-dependent signal to be small and the results can thus be used to gauge the magnitude of the background in heavy-ion collisions. Both results illustrate that these correlations are similar to those measured in heavy-ion collisions.

In this article we report results on two-particle correlations of different orders as well as various two-particle correlations relative to the second, third and fourth-order symmetry planes for charged particles in Pb–Pb collisions at $\sqrt{s_{\text{NN}}} = 2.76$ and 5.02 TeV. The motivation for utilising different planes is that the charge separation originating from the CME is expected to be present along the direction of the magnetic field and thus perpendicular to the reaction plane, approximated by Ψ_2 . Since the third order symmetry plane Ψ_3 is very weakly correlated with Ψ_2 [37] the charge separation effect relative to the third harmonic symmetry plane is expected to be negligible. First results on correlations relative to Ψ_3 have been reported by the CMS Collaboration in Ref. [38], indicating that the charge separation could be originating from the coupling of two-particle correlations with the anisotropic flow. In addition, contributions from correlations induced by the CME should be strongly suppressed in the measurements of two-particle correlations relative to Ψ_4 , while the background effects stemming from local charge conservation should scale with v_4 [39]. Therefore, measurements of correlations relative to higher order symmetry planes are expected to reflect mainly, if not solely, background effects.

The article is organised as follows: Sec. 2 describes briefly the experimental setup, while Sec. 3 discusses the data sample, the selection criteria as well as the correlators reported; these sections are followed by Sec. 4 and Sec. 5 where the estimation of the systematic uncertainties of all measurements and the main physics results, respectively, are presented. We conclude in Sec. 6 with a summary.

2 Experimental setup

By convention in ALICE, the beam direction defines the z -axis, the x -axis is horizontal and points towards the centre of the LHC, and the y -axis is vertical and points upwards. The apparatus consists of a set of detectors located in the central barrel, positioned inside a solenoidal magnet which can generate a field parallel to the beam direction with maximum magnitude of 0.5 T. A set of forward detectors completes the experimental setup.

The main tracking devices of ALICE are the Inner Tracking System (ITS) [40] and the Time Projection Chamber (TPC) [41]. The ITS consists of six cylindrical layers of silicon detectors employing three different technologies. The two innermost layers, positioned at $r = 3.9$ cm and 7.6 cm, are Silicon Pixel Detectors (SPD), followed by two layers of Silicon Drift Detectors (SDD) ($r = 15$ cm and 23.9 cm). Finally, the two outermost layers are double-sided Silicon Strip Detectors (SSD) at $r = 38$ cm and 43 cm. The TPC surrounds the ITS and provides full azimuthal coverage. The combined pseudorapidity (η) coverage of the ITS and the TPC is $-0.9 < \eta < 0.9$.

A set of forward detectors, the V0 scintillator arrays [42], were used in the trigger logic and for the determination of the collision centrality, discussed in the next section. The V0 consists of two sub-systems, the V0A and the V0C, that are positioned on either side of the interaction point and cover the pseudorapidity ranges of $2.8 < \eta < 5.1$ and $-3.7 < \eta < -1.7$, respectively. Finally the Zero Degree Calorimeters (ZDC) [40] positioned at both positive and negative rapidity at around 114 m away from the interaction point were also used offline to reduce the contamination from beam-induced background.

A detailed description of ALICE and its sub-detectors can be found in Ref. [40] and their performance in Ref. [43].

3 Analysis details

3.1 Event and track selection

The analysis is performed using the Pb–Pb data samples collected in 2010 and 2015 at a centre-of-mass energy per nucleon pair of $\sqrt{s_{NN}} = 2.76$ and 5.02 TeV, respectively. The minimum bias trigger condition is defined in the 2010 data sample by combinations of hits in the SPD and either V0A or V0C detectors, while in 2015 the trigger required a signal in both V0A and V0C detectors.

An offline event selection relying on the timing information from the V0 and the neutron ZDC is used to reject beam-gas background and parasitic beam-beam interactions. Events are analysed if the z -coordinate of the reconstructed primary vertex (V_z) resides within ± 10 cm from the nominal interaction point. The collision centrality is estimated from the amplitude of the signal measured by the V0 detectors as explained in Ref. [44]. Higher amplitude, and hence higher particle multiplicity, corresponds to more central (smaller impact parameter) events. The data sample is divided into centrality classes which span 0–70% of the inelastic hadronic cross section, which is considered in this study. The 0–5% and 60–70% intervals correspond to the most central and the most peripheral collisions, respectively.

Charged particles reconstructed using the TPC and the ITS information are accepted for analysis within η and p_T ranges of $|\eta| < 0.8$ and $0.2 < p_T < 5$ GeV/ c , respectively. The tracking algorithm, based on the Kalman filter [45, 46], starts from a collection of space points (referred to as clusters) inside the TPC, and provides the quality of the fit by calculating its χ^2 value. The track parameters at the primary vertex are then updated using the combined information from both the TPC and the ITS detectors. Tracks are accepted even if the algorithm is unable to match the track reconstructed in the TPC with associated SPD clusters (e.g. due to inefficiencies caused by dead channels in the SPD layers). In this case, a cluster from another layer of the ITS (e.g. SDD) is used to reconstruct the tracks. This tracking mode will be referred to as hybrid tracking in the rest of the text and is used as the default in this analysis since it

provides a uniform distribution in azimuthal angle (φ). More details about the tracking parameters and performance are described elsewhere [40, 43]. Accepted tracks are required to have at least 70 out of 159 possible space points measured in the TPC and a χ^2 per degree of freedom of the momentum fit per TPC cluster to be below 2. These selections reduce the contribution from short tracks, which are unlikely to originate from the primary vertex. To further reduce the contamination by secondary tracks from weak decays or from the interaction with the material, only tracks within a maximum distance of closest approach (DCA) to primary vertex in both the transverse plane ($\text{DCA}_{xy} < 2.4$ cm) and the longitudinal direction ($\text{DCA}_z < 3.2$ cm) were considered. Moreover, if matched to ITS clusters, the tracks are required to have at least one cluster in either of the two SPD layers. These selections lead to an efficiency of about 65% for primary tracks at $p_T = 0.5$ GeV/c, which reaches 80% above 1 GeV/c. The variation of these values between central and peripheral collisions is less than 3%, and does not change between $\sqrt{s_{NN}} = 2.76$ and 5.02 TeV. The contamination from secondaries is about 10% at $p_T = 0.2$ GeV/c, reaches 5% at $p_T = 1$ GeV/c and decreases further with increasing transverse momentum.

3.2 Analysis methodology

A way to probe the P-odd leading order coefficient $a_{1,\alpha}$ that reflects the magnitude of the CME is through the study of charge-dependent two-particle correlations relative to the reaction plane Ψ_{RP} . The expression proposed in Ref. [24] is of the form $\langle \cos(\varphi_\alpha + \varphi_\beta - 2\Psi_{RP}) \rangle$ (α and β being particles with the same or opposite charges) that can probe correlations between the leading P-odd terms for different charge combinations $\langle a_{1,\alpha} a_{1,\beta} \rangle$. This can be seen if one decomposes the correlator using Eq. 1

$$\begin{aligned} \langle \cos(\varphi_\alpha + \varphi_\beta - 2\Psi_{RP}) \rangle &= \\ \langle \cos [(\varphi_\alpha - \Psi_{RP}) + (\varphi_\beta - \Psi_{RP})] \rangle &= \langle \cos(\Delta\varphi_\alpha + \Delta\varphi_\beta) \rangle = \\ \langle \cos\Delta\varphi_\alpha \cos\Delta\varphi_\beta \rangle - \langle \sin\Delta\varphi_\alpha \sin\Delta\varphi_\beta \rangle &= \langle v_{1,\alpha} v_{1,\beta} \rangle + B_{in} - \langle a_{1,\alpha} a_{1,\beta} \rangle - B_{out}, \end{aligned} \quad (2)$$

where B_{in} and B_{out} represent the parity-conserving correlations projected onto the in- and out-of-plane directions. The terms $\langle \cos\Delta\varphi_\alpha \cos\Delta\varphi_\beta \rangle$ and $\langle \sin\Delta\varphi_\alpha \sin\Delta\varphi_\beta \rangle$ in Eq. 2 quantify the correlations with respect to the in- and out-of-plane directions, respectively. The term $\langle v_{1,\alpha} v_{1,\beta} \rangle$, i.e. the product of the first order Fourier harmonics or directed flow, is expected to have negligible charge dependence in the midrapidity region [47]. In addition, for a symmetric collision system the average directed flow at midrapidity is zero. A generalised form of Eq. 2 also describing higher harmonics is given by the mixed-harmonics correlations, which reads

$$\gamma_{m,n} = \langle \cos(m\varphi_\alpha + n\varphi_\beta - (m+n)\Psi_{|m+n|}) \rangle, \quad (3)$$

where m and n are integers. Setting $m = 1$ and $n = 1$ (i.e. $\gamma_{1,1}$) leads to Eq. 2. The $|m+n|$ -th order symmetry plane angle $\Psi_{|m+n|}$ is introduced to take into account that the overlap region of the colliding nuclei exhibits an irregular shape [19–23]. This originates from the initial density profile of nucleons participating in the collision, which is not isotropic and differs from one event to the other. In case of a smooth distribution of matter produced in the overlap zone, the angle $\Psi_{|m+n|}$ coincides with that of the reaction plane, i.e. $\Psi_{|m+n|} = \Psi_{RP}$.

In order to independently evaluate the contributions from correlations in- and out-of-plane, one can also measure a two-particle correlator of the form

$$\langle \cos(\varphi_\alpha - \varphi_\beta) \rangle = \langle \cos [(\varphi_\alpha - \Psi_{RP}) - (\varphi_\beta - \Psi_{RP})] \rangle = \langle \cos(\Delta\varphi_\alpha - \Delta\varphi_\beta) \rangle =$$

$$\langle \cos \Delta \varphi_\alpha \cos \Delta \varphi_\beta \rangle + \langle \sin \Delta \varphi_\alpha \sin \Delta \varphi_\beta \rangle = \langle v_{1,\alpha} v_{1,\beta} \rangle + \mathbf{B}_{\text{in}} + \langle a_{1,\alpha} a_{1,\beta} \rangle + \mathbf{B}_{\text{out}}, \quad (4)$$

which corresponds to the special case of $m = -n$ in Eq. 3. This provides access to the two-particle correlations without any dependence on the symmetry plane angle

$$\delta_m = \langle \cos[m(\varphi_\alpha - \varphi_\beta)] \rangle. \quad (5)$$

This correlator, owing to its construction, is affected if not dominated by non-flow contributions. Charge-dependent results for δ_1 , together with the relevant measurements of $\gamma_{1,1}$ were first reported in Ref. [25] and made it possible to separately quantify the magnitude of correlations in- and out-of-plane.

In this article, we report on the charge-dependent results of four correlators of the form of Eq. 3. The first two, $\gamma_{1,1}$ and $\gamma_{1,-3}$, probe correlations of particles relative to the second order symmetry plane (Ψ_2). The correlator $\gamma_{1,1}$ (i.e. the main correlator used in previous studies) probes correlations of the first order P-odd term, i.e. $\langle a_{1,\alpha} a_{1,\beta} \rangle$ as illustrated in Eq. 2, while the second is sensitive not only to the first but also the second order coefficient, i.e. $\langle a_{1,\alpha} a_{2,\beta} \rangle$ and thus is sensitive to the magnitude and the shape of the CME contribution. However, in both cases the background contributions from local charge conservation are expected to be significant (see Ref. [31, 32] and the references therein).

In order to evaluate the background, correlations relative to the third and fourth order symmetry planes i.e., $\gamma_{1,2}$ and $\gamma_{2,2}$, are investigated. Since the charge-separation effects originating from the CME form relative to the second order symmetry plane, both correlators are expected to have negligible contribution from it. Their charge-dependent part could thus be used as a proxy for the background that consists of local charge conservation scaled by the corresponding flow harmonics according to Ref. [48]

$$\gamma_{1,1} \approx \langle \cos[(\varphi_\alpha - \varphi_\beta) + 2(\varphi_\beta - \Psi_2)] \rangle \propto \delta_1 v_2, \quad (6a)$$

$$\gamma_{1,2} \approx \langle \cos[(\varphi_\alpha - \varphi_\beta) + 3(\varphi_\beta - \Psi_3)] \rangle \propto \delta_1 v_3, \quad (6b)$$

$$\gamma_{2,2} \approx \langle \cos[2(\varphi_\alpha - \varphi_\beta) + 4(\varphi_\beta - \Psi_4)] \rangle \propto \delta_2 v_4. \quad (6c)$$

By taking the difference of results between opposite- and same-sign charge combinations, denoted as $\Delta\gamma_{mn}$ in the most general form of the correlator, one can eliminate the charge-independent part and probe the contribution from local charge conservation modulated by the relevant flow harmonic

$$\Delta\gamma_{1,1} \approx \kappa_2 v_2 \Delta\delta_1, \quad (7a)$$

$$\Delta\gamma_{1,2} \approx \kappa_3 v_3 \Delta\delta_1, \quad (7b)$$

$$\Delta\gamma_{2,2} \approx \kappa_4 v_4 \Delta\delta_2, \quad (7c)$$

where κ_n is a proportionality constant. Using Eqs. 7, one can thus estimate the contribution of the background in the charge-dependent CME sensitive correlator $\Delta\gamma_{1,1}$ using the results of e.g. $\Delta\gamma_{1,2}$ according to

$$\Delta\gamma_{1,1}^{\text{Bkg}} \approx \Delta\gamma_{1,2} \times \frac{v_2 \kappa_2}{v_3 \kappa_3}. \quad (8)$$

Equation 8 serves as a tool to disentangle the CME contribution from the background, provided the parameter κ_2/κ_3 is estimated. In Ref. [35] it was argued that the magnitude of these κ_n terms depends on the kinematic ranges (e.g. detector acceptance, event and particle selection criteria). Therefore, it was suggested that one can assume that $\kappa_2 \approx \kappa_3$ if the same kinematic conditions are used to calculate

$\Delta\gamma_{m,n}$ within the same experimental setup. In this article, we also investigate the relationship between κ_2 and κ_3 using two approaches: a blast wave [49] inspired model that incorporates effects of local charge conservation and the results of A Multi Phase Transport model (AMPT) [50–52], both discussed in detail in the Results section.

3.2.1 The event-plane method

To evaluate the correlations experimentally, the event-plane method [53, 54] is used. In this method, the event plane angle is reconstructed from the azimuthal distribution of the particles produced in a collision. The event plane angle of k -th order (where $k = |m - n|$) $\Psi_{k,EP}$ is estimated according to

$$\Psi_{k,EP} = \tan^{-1} \frac{Q_{k,y}}{Q_{k,x}}, \quad (9)$$

where $Q_{k,x}$ and $Q_{k,y}$ are the x - and y -components of the Q -vector, calculated as

$$Q_{k,x} = \sum_{i=1}^M w_i(p_T, \eta, \varphi, V_z) \cos(k\varphi_i), \text{ and } Q_{k,y} = \sum_{i=1}^M w_i(p_T, \eta, \varphi, V_z) \sin(k\varphi_i). \quad (10)$$

In Eq. 10, φ_i corresponds to the azimuthal angle of the i -th track in an event with multiplicity M . The factors $w_i(p_T, \eta, \varphi, V_z)$ are weights applied on every track in the construction of the Q -vectors, in order to correct for non-uniform reconstruction efficiency and acceptance. They are calculated as a function of the transverse momentum, pseudorapidity and azimuthal angle of particles for different V_z values of the primary vertex.

To reduce the contributions from short range effects not related to the common symmetry planes (i.e. non-flow), a subevent plane technique [53, 54] is implemented. Each event is divided into two subevents “A” and “B”, covering the ranges $-0.8 < \eta < 0$ and $0 < \eta < 0.8$, respectively, and the two subevent plane angles, namely $\Psi_{k,A}$ and $\Psi_{k,B}$ are calculated using charged particles. The correlators of Eq. 3 are then calculated as

$$\gamma_{mn} = \frac{\langle \cos[m\varphi_\alpha + n\varphi_\beta - (m+n)\Psi_{|m+n|,EP}] \rangle}{R(\Psi_{|m+n|,EP})}, \quad (11)$$

where α and β correspond to any two charged particles within $-0.8 < \eta < 0.8$, and $\Psi_{|m+n|,EP}$ corresponds to subevent plane $\Psi_{k,A}$ (or $\Psi_{k,B}$ for systematic studies). Particles α or β (or both) were excluded from the determination of event plane if they were from the same η window as the one used to calculate $\Psi_{k,A}$ or $\Psi_{k,B}$.

The event plane resolution $R(\Psi_{|m+n|,EP})$ is given by

$$R(\Psi_{|m+n|,EP}) = \sqrt{\cos[|m+n|(\Psi_{|m+n|,A} - \Psi_{|m+n|,B})]}. \quad (12)$$

4 Systematic uncertainties

The systematic uncertainties in all measurements presented in this article were estimated by varying the event and track selection criteria as well as by studying the detector effects with Monte Carlo (MC) simulations. The contributions from different sources, described below, were extracted from the difference for the results of each correlator obtained with the primary selection criteria and the ones after the relevant variation was applied. All sources with a difference between the results larger than 1σ were then added in quadrature to form the final value of the systematic uncertainty (for each data point), where σ is the

uncertainty of the difference between the default results and the ones obtained from the variation of the selection criteria, taking into account the degree of their correlation [55].

Table 1 summarises the sources and the variations that were tested. In particular, the systematic uncertainty originating from the selection of the z position of the primary vertex was investigated by changing this selection from ± 10 cm down to ± 8 cm. In order to estimate the contribution to the results from the choice of the detector used as centrality estimator, the analysis was performed using the number of hits in the second layer of the SPD instead of the amplitude of the V0 detector. Furthermore, data samples recorded with different magnetic field configurations for the solenoid magnet were analysed separately. The contribution of residual pile-up events to the results was estimated by analysing independently the high and low interaction rate samples. Finally, the results were obtained separately by calculating the event plane from different pseudorapidity ranges within the TPC acceptance. The systematic uncertainty in the extraction of the CME fraction when using different event plane angles within the TPC acceptance for the highest LHC energy was estimated considering runs with low beam intensity where the distortions in the TPC are negligible.

In parallel, to investigate any potential bias originating from the quality of the tracks used in the analysis, the number of space points measured in the TPC was varied from 70 (default) up to 100 out of 159 maximum points that a track can have. The contribution stemming from secondary tracks, either from weak decays or from the interaction of particles with the detector material, was investigated by tightening the selection on the DCA in the longitudinal direction as well as in the transverse plane. Finally, another tracking mode that relies on the combination of the TPC and the ITS detectors, henceforth called global tracking, with tighter selection criteria in addition to requirements for clusters in the SPD or the SDD detectors was used. In this case, a stricter transverse momentum dependent requirement in the value of the DCA in the transverse plane resulted in reducing even further the amount of secondary particles in the track sample. The resulting contamination from secondaries is less than 2–3% for the entire p_T range.

For each variation, new correction maps for detector inefficiencies and non-uniform acceptance were extracted using MC data samples and collision data.

Table 1: List of the selection criteria and the corresponding variations used for the estimation of the systematic uncertainties.

(No.) Source	Default Value	Variations
(1) Primary V_z	± 10 cm	± 8 cm
(2) Centrality Estimator	V0 amplitude	SPD cluster
(3) Magnetic field polarity	Combined	Positive, Negative
(4) Event plane	$\Psi_{k,-0.8 < \eta < 0}$	$\Psi_{k,0 < \eta < 0.8}$
(5) Residual Pile-Up	High Intensity data	Low Intensity data
(6) TPC space points	70	100
(7) DCA_{xy} (DCA_z)	2.4 (3.2) cm	2.0 (2.0) cm
(8) Tracking Algorithm	Hybrid	Global
(9) Charge Combination	“++” and “--” combined	“++” or “--”

Tables 2 and 3 summarise the maximum magnitude, over all centrality intervals, of the systematic uncertainties from each individual source for all correlators presented in this article. The uncertainties are reported separately for the results for same-sign (SS), opposite-sign (OS) and the difference between opposite- and same-sign (OS-SS) pairs. The uncertainties for the results of the various $\gamma_{m,n}$ are reported without the common factor of $\times 10^{-5}$.

Throughout the centrality intervals reported in this article, the magnitude of $\gamma_{1,1}$ correlator varies between -2.4 to -40 for SS pair, -1.2 to 29 for OS pair and 1.2 to 68 for OS-SS. The values of $\gamma_{1,-3}$ vary between

-2.1 to 38 for SS pair, -0.67 to 68 for OS pair and 1.4 to 30 for OS-SS. The magnitude of $\gamma_{1,2}$ covers the range between -2.5 to 140 for SS pair, -1.7 to 180 for OS pair and 0.71 to 3.7 for OS-SS. Finally, the results for $\gamma_{2,2}$ vary between 0.01 to 14.7 for SS and OS pair while being between 0.25 and 19 for OS-SS.

The two-particle correlators of the form δ_m are an order of magnitude larger than the three-particle correlators. Therefore, the values mentioned in the following have an exponent of $\times 10^{-4}$. The magnitude of δ_1 varies between 2.9 to 23.5 for SS pair, 5.6 to 49 for OS pair and 2.7 to 26.2 for OS-SS. The values of δ_2 spans the range between 8.2 to 97 for SS pair, 9.5 to 102 for OS pair and 1.31 to 5.2 for OS-SS. The magnitude of δ_3 varies between 4.5 to 16 for SS pair, 4.8 to 15 for OS pair and -1.3 to 0.79 for OS-SS. Finally, the results for δ_4 varies between 1.58 to 9.4 for SS pair, 1.6 to 6.8 for OS pair and -2.5 to 0.78 for OS-SS.

Table 2: Maximum systematic uncertainty (absolute value) over all centrality intervals on γ_{mn} from individual sources (see Tab. 1 for an explanation of each source). The ranges are similar for both energies.

Sources	$\gamma_{1,1} (\times 10^{-5})$			$\gamma_{1,2} (\times 10^{-5})$			$\gamma_{1,-3} (\times 10^{-5})$			$\gamma_{2,2} (\times 10^{-5})$		
	SS	OS	OS-SS	SS	OS	OS-SS	SS	OS	OS-SS	SS	OS	OS-SS
(1)	0.26	1.4	0.027	1.1	0.12	1.9	0.13	0.15	0.095	0.035	0.1	0.02
(2)	2.5	6.1	6	4.5	9.9	1.8	4.2	3.2	1.2	8.6	8.6	0.27
(3)	0.86	0.65	0.1	0.83	0.84	0.024	0.34	0.54	0.04	1.4	0.98	0.36
(4)	1.62	1.81	1.6	1.7	1.83	4.51	0.86	0.64	0.15	1.78	2.1	6.8
(5)	4.0	3.9	0.58	7.2	3.9	3.6	0.73	0.83	0.2	4.4	4.0	11
(6)	0.1	0.89	0.065	1.1	1.4	1.3	0.21	0.22	0.032	4.1	3.9	0.12
(7)	0.011	0.032	0.001	0.05	0.06	2.1	0.008	0.024	0.025	0.017	0.28	0.03
(8)	0.045	0.049	0.16	0.67	1.3	0.08	0.07	0.06	0.17	5.7	0.17	0.1
(9)	0.55	-	0.55	0.26	-	0.26	0.23	-	0.23	21	-	21

Table 3: Maximum systematic uncertainty (absolute value) over all centrality intervals on δ_m from individual sources (see Tab. 1 for an explanation of each source). The ranges are similar for both energies.

Sources	$\delta_1 (\times 10^{-4})$			$\delta_2 (\times 10^{-4})$			$\delta_3 (\times 10^{-4})$			$\delta_4 (\times 10^{-4})$		
	SS	OS	OS-SS									
(1)	1.7	1.8	0.01	0.12	0.13	0.03	0.08	0.11	0.03	0.06	0.05	0.01
(2)	2.0	3.6	1.6	0.65	0.66	0.019	0.5	0.11	0.34	0.43	0.17	0.27
(3)	0.86	1.0	0.35	1.6	1.4	0.25	0.64	0.22	0.33	0.52	0.02	0.51
(5)	1.2	0.91	1.5	1.4	0.99	0.029	0.89	0.38	0.33	0.61	0.13	0.022
(6)	0.014	2.2	1.4	5.5	5.5	1.1	0.26	1.1	1.1	0.94	2.2	0.12
(7)	0.056	0.15	0.01	0.08	0.14	0.01	0.05	0.02	0.02	0.14	0.02	0.07
(8)	2.5	1.8	0.74	0.92	0.29	1.2	1.2	0.53	1.8	0.68	0.67	1.4
(9)	2.6	-	2.6	1.6	-	1.6	1.7	-	1.7	0.37	-	0.37

5 Results

The measurements of two-particle correlators (Eq. 5) are presented in Fig. 1. Each data point on this figure and in the rest of the article is drawn with the relevant statistical (vertical lines) and systematic uncertainties (shaded boxes). The plots in the left panel of Fig. 1 present the centrality dependence of δ_m for $m = 1, 2, 3$ and 4 for opposite (OS) and same (SS) sign pairs. The charge-dependent differences of every correlator, denoted by $\Delta\delta_1$, $\Delta\delta_2$, $\Delta\delta_3$, and $\Delta\delta_4$ as a function of collision centrality are presented in the right panel of Fig. 1. These charge-dependent two-particle correlators (Eq. 5) are primarily dominated by background effects (see discussion in Section 3) and can thus be used to constrain the background in the CME sensitive correlator $\gamma_{1,1}$. The first harmonic correlator, δ_1 , exhibits a significant charge-dependent difference. This correlator is related to the balance function also studied at the LHC [56, 57].

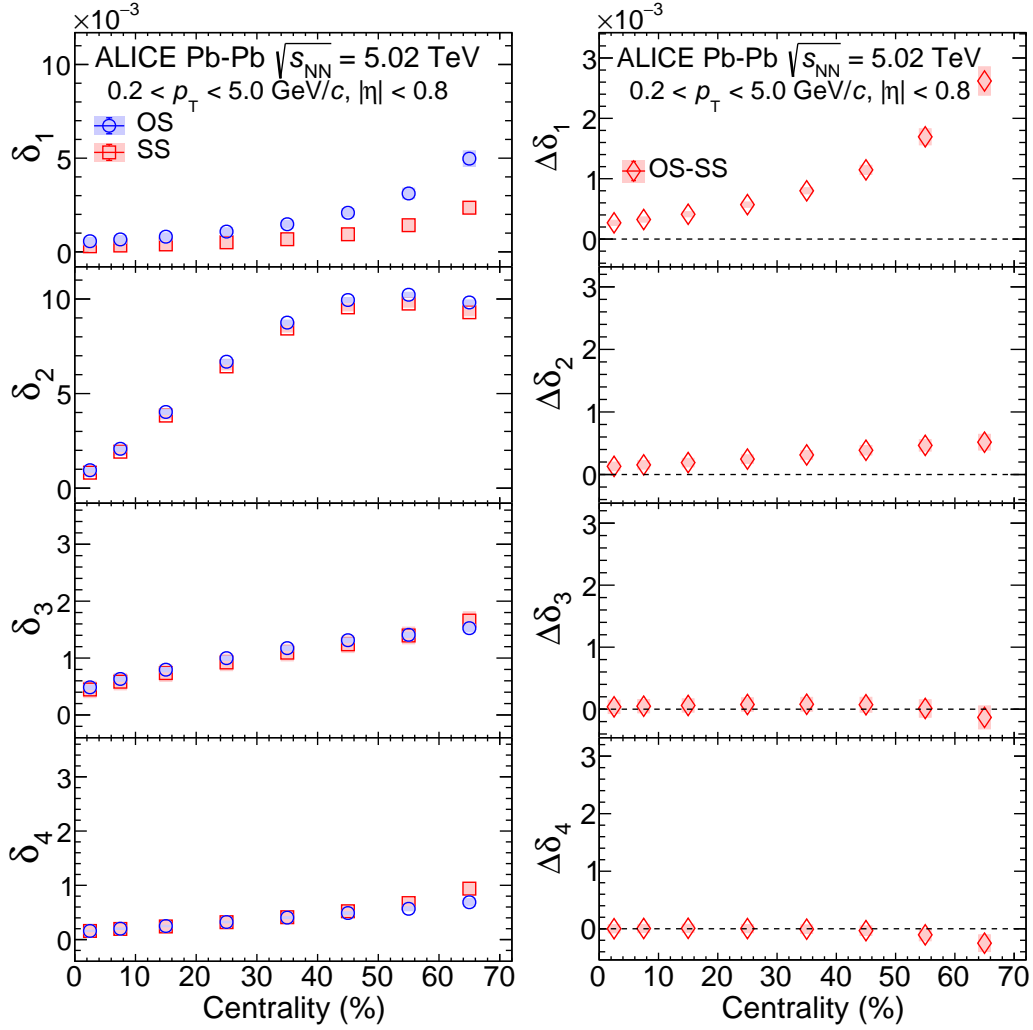


Figure 1: (Left panel): The centrality dependence of δ_1 , δ_2 , δ_3 , and δ_4 for pairs of particles of opposite (OS) and same (SS) sign measured in Pb–Pb collisions at $\sqrt{s_{\text{NN}}} = 5.02$ TeV. (Right panel): The charge-dependent differences, $\Delta\delta_n$ for $n = 1, 2, 3$ and 4, as a function of collision centrality. The statistical uncertainties for some data points are smaller than the marker size. The systematic uncertainties of each data point are represented by the shaded boxes.

The present results are qualitatively consistent with the ones in Refs. [56] and [57], i.e. oppositely charged particles are more tightly correlated in central events resulting in a narrowing of the balance function width in $\Delta\phi$ and thus in a smaller value of δ_1 for central events compared to peripheral Pb–Pb collisions. For higher harmonics, the charge-dependent differences become progressively smaller and are compatible with zero (up to centrality $\leq 60\%$) with a hint of negative $\Delta\delta_4$ for the most peripheral events.

The two-particle correlators were also studied in a more differential way, namely as a function of the transverse momentum difference $\Delta p_{\text{T}} = |p_{\text{T},\alpha} - p_{\text{T},\beta}|$, the average transverse momentum $\bar{p}_{\text{T}} = (p_{\text{T},\alpha} + p_{\text{T},\beta})/2$ and the pseudorapidity difference $\Delta\eta = |\eta_{\alpha} - \eta_{\beta}|$ of the pair.

The dependence of δ_1 , δ_2 , δ_3 and δ_4 on these variables for one indicative centrality interval (30–40%) is shown in Fig. 2 for Pb–Pb collisions at $\sqrt{s_{\text{NN}}} = 5.02$ TeV. For the first harmonic correlator, δ_1 , the correlations between particles of opposite charges have larger magnitude compared with the ones for same charge particles. The absolute differences do not show any significant Δp_{T} dependence, however they do

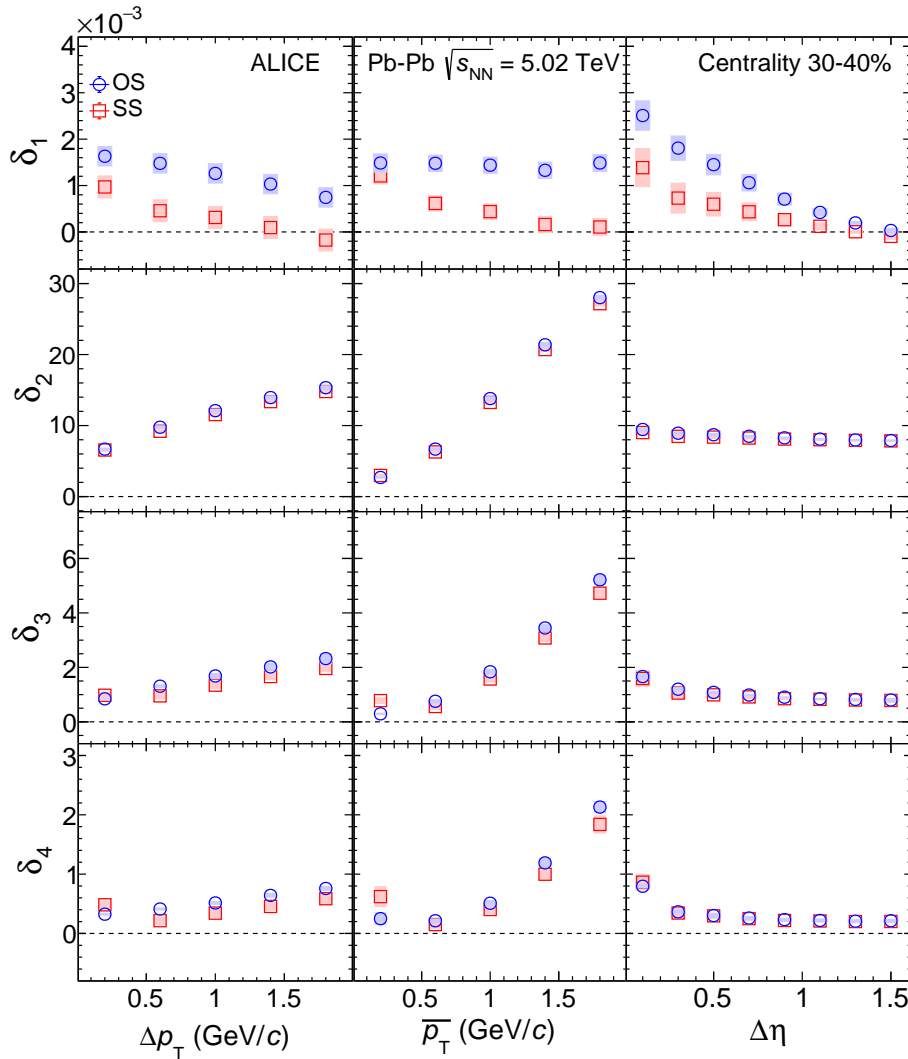


Figure 2: The dependence of δ_1 , δ_2 , δ_3 and δ_4 on the transverse momentum difference $\Delta p_T = |p_{T,\alpha} - p_{T,\beta}|$ (left panel), the average transverse momentum $\bar{p}_T = (p_{T,\alpha} + p_{T,\beta})/2$ (middle panel) and the pseudorapidity difference $\Delta\eta = |\eta_\alpha - \eta_\beta|$ (right panel) of the pair. The results for both opposite (circles) and same sign (squares) particle pairs are reported for one indicative centrality interval (30–40%) of Pb–Pb collisions at $\sqrt{s_{NN}} = 5.02$ TeV.

increase with increasing \bar{p}_T of the pair. Finally, there is a significant charge-dependent difference of δ_1 , which decreases with increasing $\Delta\eta$, consistent with what is also reported in Ref. [56, 57]. For higher harmonics, no significant difference is observed. For other centralities the results look qualitatively similar.

The measurements of integrated two-particle correlators relative to various order symmetry planes (Eq. 3) in Pb–Pb collisions at $\sqrt{s_{NN}} = 5.02$ TeV are presented in Fig. 3. The left panel presents the centrality dependence of $\gamma_{1,1}$, $\gamma_{1,-3}$, $\gamma_{1,2}$ and $\gamma_{2,2}$. Results for different charge combinations, i.e. OS and SS pairs are also presented here. The right panel of the same figure presents the centrality dependence of the charge-dependent differences, i.e. OS-SS. A significant charge-dependent magnitude for $\gamma_{1,1}$ is observed that increases when moving to more peripheral collisions. In particular, the magnitude of the same-sign correlations becomes progressively more negative, while correlations of oppositely charged particles are very close to zero and their magnitude turns positive for peripheral Pb–Pb events. A significant charge-dependent difference that increases for peripheral centrality intervals is also observed for $\gamma_{1,-3}$. Both correlators, as discussed in Sec. 3, probe correlations between either the first order P-odd term of the

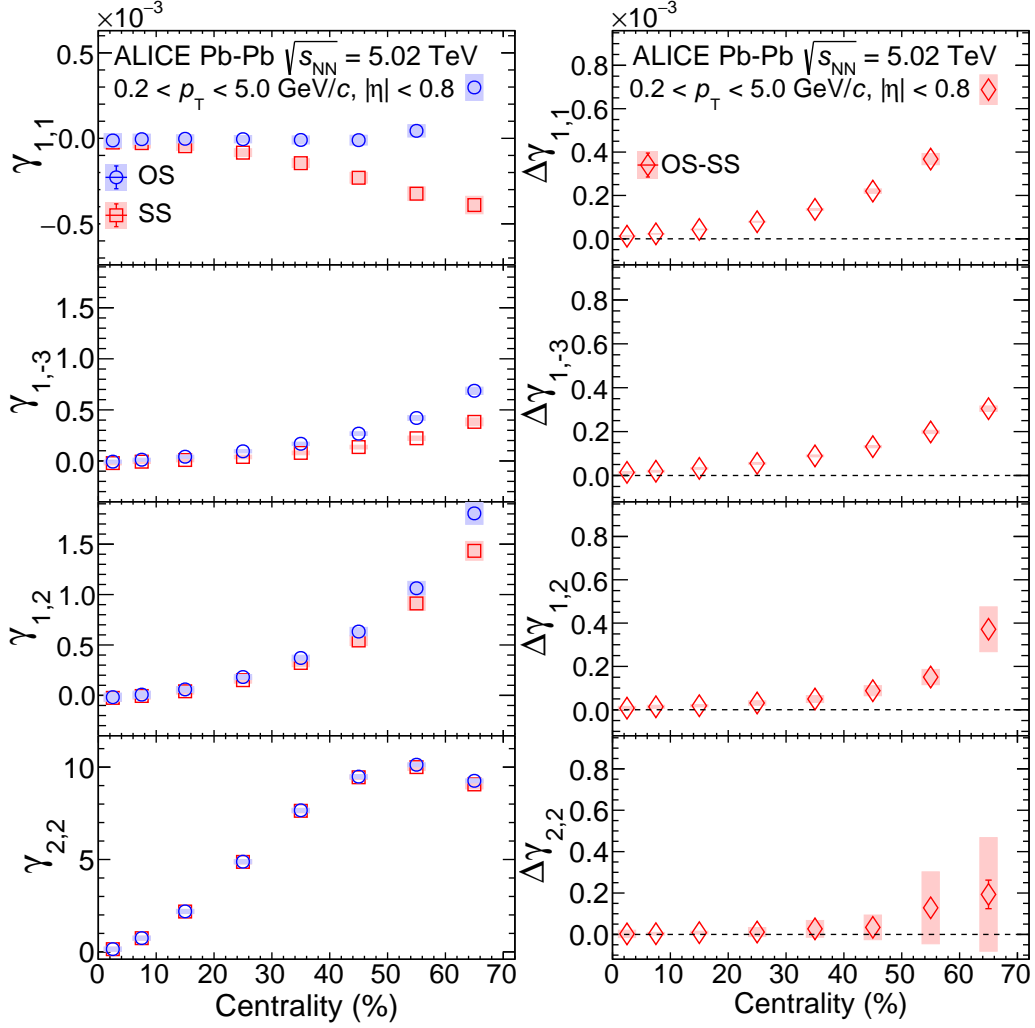


Figure 3: (Left panel): The centrality dependence of $\gamma_{1,1}$, $\gamma_{1,-3}$, $\gamma_{1,2}$ and $\gamma_{2,2}$ for pairs of particles of opposite (OS) and same (SS) sign measured in Pb–Pb collisions at $\sqrt{s_{NN}} = 5.02$ TeV. (Right panel): The charge-dependent differences $\Delta\gamma_{1,1}$, $\Delta\gamma_{1,-3}$, $\Delta\gamma_{1,2}$ and $\Delta\gamma_{2,2}$ as a function of collision centrality.

form $\langle a_{1,\alpha} a_{1,\beta} \rangle$ or between the first and the second order coefficient $\langle a_{1,\alpha} a_{2,\beta} \rangle$. They are thus sensitive to contributions from the CME.

The centrality dependence of $\gamma_{1,2}$ for SS and OS pairs and their difference also demonstrate a significant charge dependence which increases for more peripheral events. Correlations of particles relative to the third order symmetry plane are expected to probe solely the background scaled by the third order flow harmonic (v_3) as expressed in Eqs. 6. Hence these results indicate that the effects of local charge conservation coupled with v_3 can induce differences in correlations between different charges. Finally, correlations of particles with different charge relative to the fourth order symmetry plane, as quantified by $\gamma_{2,2}$, do not exhibit any significant charge dependence within the current level of statistical and systematic uncertainties.

As in the case of the two-particle correlators, δ_m , also the $\gamma_{m,n}$ were studied in a differential way, namely as a function of Δp_T , \bar{p}_T and $\Delta\eta$. The results are presented in Fig. 4 for the same representative centrality interval as before (30–40%) for both OS and SS. It is seen that, with the exception of $\gamma_{2,2}$, the magnitude of correlations for OS pairs is greater than the one of SS for nearly the full range of Δp_T , \bar{p}_T and $\Delta\eta$ presented in this article. The results for OS and SS are compatible within the current level of statistical

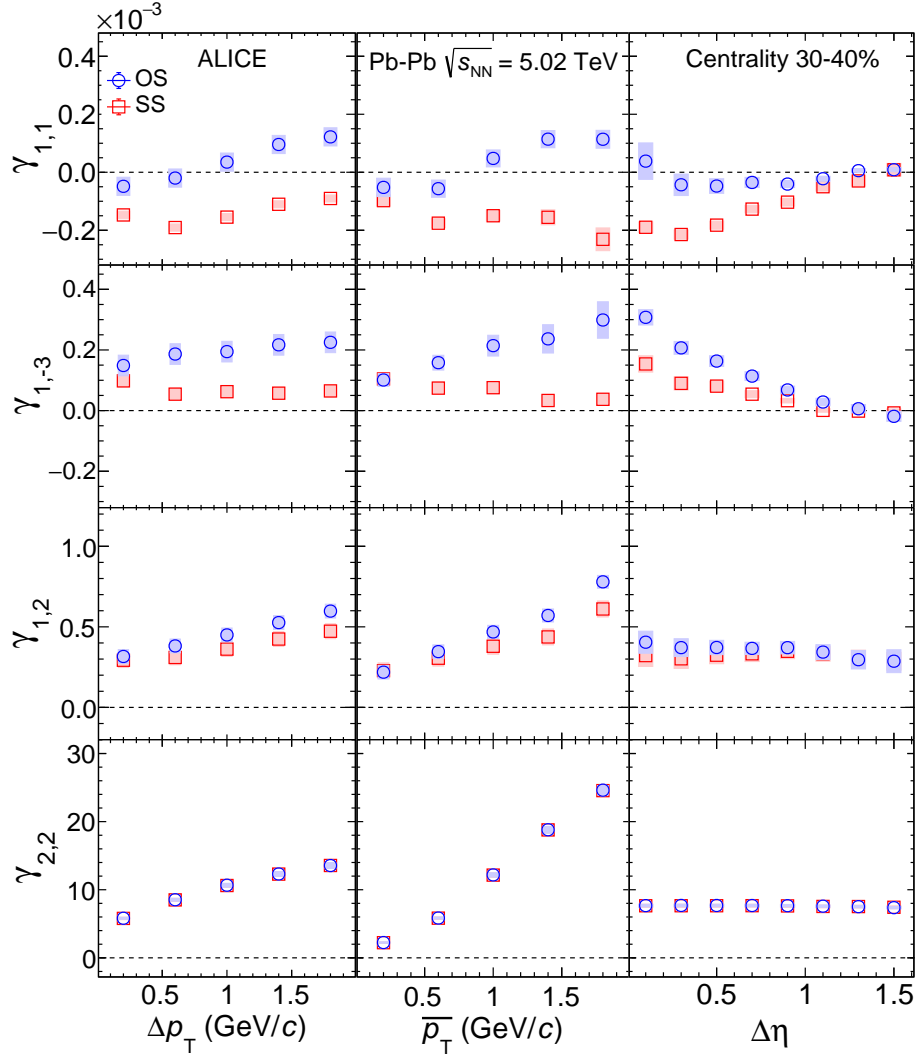


Figure 4: The dependence of $\gamma_{1,1}$, $\gamma_{1,-3}$, $\gamma_{1,2}$ and $\gamma_{2,2}$ on the transverse momentum difference $\Delta p_T = |p_{T,\alpha} - p_{T,\beta}|$ (left panel), the average transverse momentum $\bar{p}_T = (p_{T,\alpha} + p_{T,\beta})/2$ (middle panel) and the pseudorapidity difference $\Delta\eta = |\eta_\alpha - \eta_\beta|$ (right panel) of the pair. The results for both opposite and same sign particle pairs are reported for one indicative centrality interval (30–40%) of Pb–Pb collisions at $\sqrt{s_{NN}} = 5.02$ TeV.

and systematic uncertainties for $\gamma_{2,2}$.

The correlations of particles with different charge for both $\gamma_{1,1}$ and $\gamma_{1,-3}$, i.e. the two correlators that are sensitive to different orders of the CME, have a range that extends up to one unit of $\Delta\eta$. Both OS and SS correlations have a similar trend as a function of Δp_T and $\Delta\eta$, however they exhibit different behaviour as a function of \bar{p}_T . On the other hand, the correlators that are solely sensitive to the background, i.e. $\gamma_{1,2}$ and $\gamma_{2,2}$, exhibit an increasing trend as a function of both Δp_T and \bar{p}_T . This trend has a mild charge dependence for $\gamma_{1,2}$ that increases with increasing Δp_T and \bar{p}_T , but not for $\gamma_{2,2}$. Both $\gamma_{1,2}$ and $\gamma_{2,2}$ have a range that extends up to $\Delta\eta = 1.6$ without any significant dependence on $\Delta\eta$.

Finally, the charge-dependent differences of the correlators $\gamma_{1,1}$, $\gamma_{1,2}$ and $\gamma_{2,2}$ were also studied in Pb–Pb collisions at $\sqrt{s_{NN}} = 2.76$ TeV. The centrality dependence of $\Delta\gamma_{1,1}$, $\Delta\gamma_{1,2}$ and $\Delta\gamma_{2,2}$ is presented in Fig. 5 in comparison with the results obtained in Pb–Pb collisions at $\sqrt{s_{NN}} = 5.02$ TeV. None of the correlators exhibit any significant differences between the two energies, within the current level of uncertainties. This could be explained considering that there is no significant energy dependence in the effects that

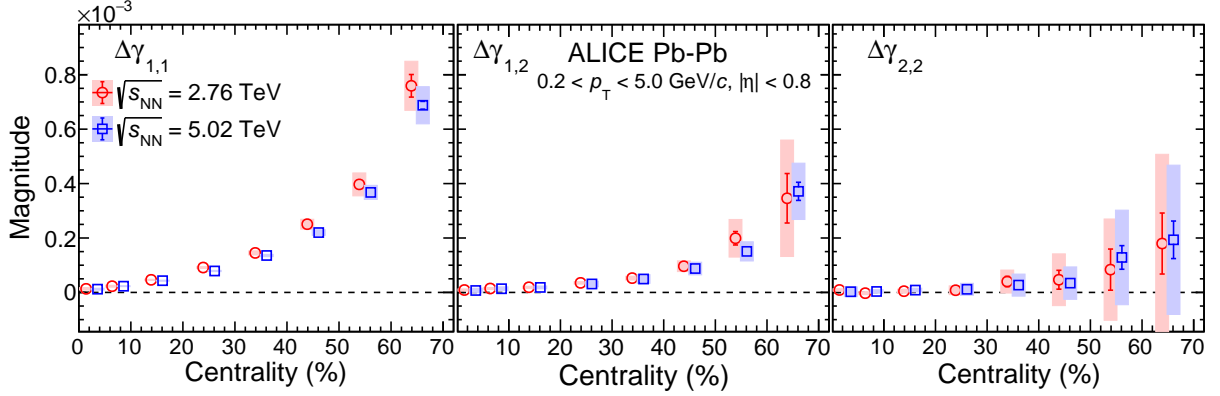


Figure 5: The dependence of $\Delta\gamma_{1,1}$, $\Delta\gamma_{1,2}$ and $\Delta\gamma_{2,2}$ on centrality, measured in Pb–Pb collisions at $\sqrt{s_{\text{NN}}} = 2.76$ and 5.02 TeV. The data points for $\sqrt{s_{\text{NN}}} = 5.02$ TeV are shifted along the horizontal axis for better visibility.

constitute the background to these measurements (i.e. local charge conservation coupled to different flow harmonic modulations). Preliminary studies indicate that the correlations between balancing charges, as reflected in the width of the balance function, do not exhibit any significant dependence on collision energy. The values of v_2 , v_3 and v_4 in $\sqrt{s_{\text{NN}}} = 5.02$ TeV are between 2 to 20% higher than the values at $\sqrt{s_{\text{NN}}} = 2.76$ TeV [58]. However, the corresponding change in the background contribution to the $\gamma_{m,n}$ correlator is of the order of a few percent, which is not distinguishable within the current level of uncertainties.

5.1 Constraining the CME contribution

5.1.1 Describing the background with Blast-wave inspired LCC model

As a first approach to constraining the CME contribution, a blast-wave (BW) parametrisation [49] that describes the phase space density at kinetic freeze-out, is used. This model assumes that the radial expansion velocity is proportional to the distance from the centre of the system and takes into account resonance production and decays. Local charge conservation (LCC) is additionally incorporated in this model by generating ensembles of particles with zero net charge. The position of the sources of balancing charges are then uniformly distributed within an ellipse. From now on this model will be denoted as BW-LCC in the text.

Table 4: List of the Blast-wave fit parameters.

Centrality	T_{kin} (MeV)	ρ_0	ρ_2	R_x/R_y
0–5%	91.3 ± 3.5	1.26 ± 0.01	0.020 ± 0.001	0.956 ± 0.001
5–10%	87.0 ± 3.5	1.27 ± 0.01	0.032 ± 0.001	0.933 ± 0.002
10–20%	84.8 ± 4.9	1.25 ± 0.01	0.045 ± 0.003	0.905 ± 0.004
20–30%	87.4 ± 4.8	1.23 ± 0.01	0.059 ± 0.007	0.872 ± 0.005
30–40%	91.6 ± 3.8	1.20 ± 0.01	0.068 ± 0.003	0.844 ± 0.004
40–50%	95.1 ± 3.3	1.15 ± 0.01	0.070 ± 0.003	0.823 ± 0.004
50–60%	98.1 ± 3.2	1.09 ± 0.01	0.065 ± 0.002	0.807 ± 0.004
60–70%	108.0 ± 3.2	0.99 ± 0.01	0.056 ± 0.002	0.786 ± 0.006

Each particle of an ensemble is emitted by a fluid element with a common collective velocity following the single-particle BW parametrisation. The procedure starts from obtaining BW parameters by fitting the p_{T} spectra [59] and the p_{T} -differential v_2 values [60] for charged pions, kaons, and protons (antipro-

tons) measured in Pb–Pb collisions at $\sqrt{s_{\text{NN}}} = 5.02$ TeV. The fit ranges for p_{T} spectra are $0.5 \leq p_{\text{T}} \leq 1.0$ GeV/ c , $0.2 \leq p_{\text{T}} \leq 1.5$ GeV/ c and $0.2 \leq p_{\text{T}} \leq 3.0$ GeV/ c for pions, kaons and protons, respectively. The fit range for p_{T} -differential v_2 and v_4 is $0.5 \leq p_{\text{T}} \leq 1.2$ GeV/ c . Table 4 presents the resulting BW parameters, namely the kinetic freezeout temperature (T_{kin}), radial flow (ρ_0) and its second order modulation (ρ_2) as well as the spacial asymmetry (R_x/R_y). The next step required tuning the number of sources of balancing pairs for each centrality interval to reproduce the centrality dependence of $\Delta\delta_1$, the correlator which is mainly sensitive to background effects. This procedure is repeated for every centrality interval. The number of sources varies from ~ 2476 to 193 for the centrality intervals 0–5% to 60–70%. The left panel of Fig. 6 presents the agreement achieved between the measured results and the ones obtained from the model. Overall the model describes the measurement fairly well with deviations limited to $< 1\%$ for the whole centrality range. The tuned model is then used to extract the expectation for the centrality dependence of the charge-dependent differences of the CME sensitive correlator $\Delta\gamma_{1,1}$. The right panel of Fig. 6 shows the comparison between the measured values of $\Delta\gamma_{1,1}$ and estimates from the model. The estimate of $\Delta\gamma_{1,1}$ from the model originates solely from the contribution of local charge conservation effects coupled to elliptic flow modulations. The curve underestimates the measured data points by as much as $\approx 39\%$, with the disagreement increasing progressively for more peripheral events.

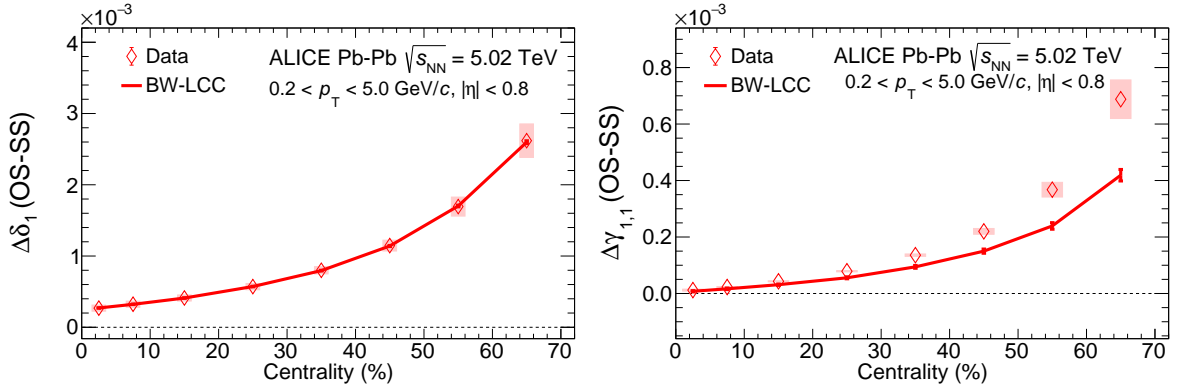


Figure 6: (Left) The centrality dependence of $\Delta\delta_1$ measured in Pb–Pb collisions at $\sqrt{s_{\text{NN}}} = 5.02$ TeV. The curve (denoted as BW-LCC) presents the blast-wave parametrization coupled to local charge conservation effects. The model is tuned to reproduce the measured values of $\Delta\delta_1$ (see text for details). (Right) The comparison of the centrality dependence of the CME-sensitive correlator $\Delta\gamma_{1,1}$ with expectations from the BW-LCC model.

5.1.2 Describing the background with v_n and $\gamma_{m,n}$

In the following, we attempt to constrain the background contribution to the CME sensitive correlator $\gamma_{1,1}$ and thus give an estimation of the fraction of the signal in Pb–Pb collisions. The approach described in Sec. 3.2 relies on the assumption that the coefficients κ_n have similar magnitude, allowing one to calculate the background contribution to $\Delta\gamma_{1,1}$, denoted as $\Delta\gamma_{1,1}^{\text{Bkg}}$ from $\Delta\gamma_{1,2}$ according to Eq. 8. This assumption was tested using events produced with the string melting tune of A Multi Phase Transport model (AMPT) [50–52]. In the string melting tune, the initial strings are melted into partons whose interactions are described by a parton cascade model [61]. These partons are then combined into final-state hadrons via a quark coalescence model. In this model, the final-state hadronic rescattering is implemented including resonance decays as well. The input parameters $\alpha_s = 0.33$ and a partonic cross section of 1.5 mb were used to reproduce the centrality dependence of v_2 and v_3 for charged particles, as reported in Ref. [62], for Pb–Pb events at $\sqrt{s_{\text{NN}}} = 2.76$ TeV. About 40 million simulated Pb–Pb events were analysed, split into centrality based on the values of the impact parameter. Only primary particles having the same kinematic selections as in the experimental data (i.e. $|\eta| < 0.8$ and $0.2 < p_{\text{T}} < 5$ GeV/ c) were considered. The left panel of Fig. 7 presents the ratio of the charge-dependent differences $\Delta\gamma_{1,1}$ and $\Delta\gamma_{1,2}$ to the relevant harmonics v_2 and v_3 , respectively. Similar ratios are also shown from the BW-LCC

model, which is discussed in the previous subsection. The two sets of data points are compatible within uncertainties over the entire centrality range for both AMPT and BW-LCC model. This is also illustrated in the right panel of Fig. 7, which presents the centrality dependence of $(\Delta\gamma_{1,1}/v_2) - (\Delta\gamma_{1,2}/v_3)$, denoted as $\Delta(\Delta\gamma/v_n)$. The corresponding data points from AMPT and BW-LCC are fitted with a constant function, which yields a result compatible with zero within the uncertainties of the fit i.e., $\Delta(\Delta\gamma/v_n) = (9.4 \pm 5.5) \times 10^{-5}$ and $(5.4 \pm 14.8) \times 10^{-5}$ respectively. This observation illustrates that within these models one can assume $\kappa_2 \approx \kappa_3$. Results presented in this article have been also reproduced using the AMPT version reported in [63].

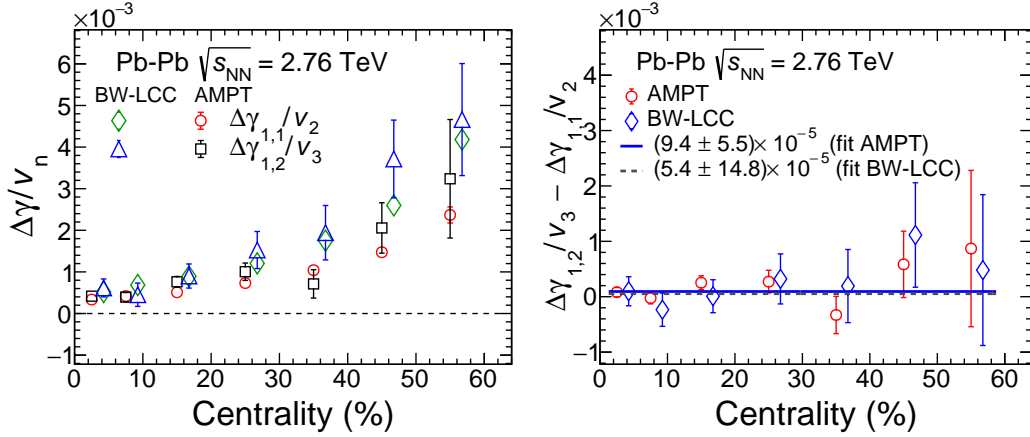


Figure 7: (Left panel) The centrality dependence of $\Delta\gamma_{1,1}/v_2$ and $\Delta\gamma_{1,2}/v_3$ for Pb–Pb collisions at $\sqrt{s_{NN}} = 2.76$ TeV according to the AMPT and BW-LCC model. (Right panel) The differences between $\Delta\gamma_{1,1}/v_2$ and $\Delta\gamma_{1,2}/v_3$ in AMPT and BW-LCC, denoted as $\Delta(\Delta\gamma/v_n)$. The solid and dotted line is the result of a fit with a constant function to AMPT and BW-LCC result respectively.

The same procedure was used with Pb–Pb data recorded at both LHC energies. Since the results of $\gamma_{2,2}$ do not give any significant charge-dependent difference as a function of centrality within statistical and systematic uncertainties (see Fig. 3), only the values of $\gamma_{1,2}$ are used in the rest of the article to estimate the background. The values of v_2 and v_3 used to scale the charge-dependent differences of $\gamma_{1,1}$ and $\gamma_{1,2}$, are the ones measured by ALICE in Pb–Pb collisions reported in Ref. [62] and Ref. [58] for $\sqrt{s_{NN}} = 2.76$ TeV and $\sqrt{s_{NN}} = 5.02$ TeV, respectively. The value of v_2 is estimated as the average of $v_2\{2\}$ and $v_2\{4\}$ to reduce the biases due to fluctuations assuming a Gaussian probability distribution [64]. Assuming $\kappa_2 \approx \kappa_3$ as supported by the model study, the value of $\Delta\gamma_{1,2} \times v_2/v_3$ was used according to Eq. 8 as a proxy for the magnitude of the background contribution to the measurement of $\Delta\gamma_{1,1}$, denoted as $\Delta\gamma_{1,1}^{\text{Bkg}}$, for both LHC energies. The CME fraction is then defined as

$$f_{\text{CME}} = 1 - \frac{\Delta\gamma_{1,1}^{\text{Bkg}}}{\Delta\gamma_{1,1}}, \quad (13)$$

where $\Delta\gamma_{1,1}$ is the measured value of the correlator presented on the left panel of Fig. 5. Figure 8 presents the centrality dependence of the CME fraction at $\sqrt{s_{NN}} = 2.76$ TeV (left plot) and $\sqrt{s_{NN}} = 5.02$ TeV (right plot). The systematic uncertainties on f_{CME} have been estimated from the same sources as mentioned in Sec. 4. In addition, the contribution to the systematic uncertainty stemming from v_2 was also estimated using $v_2\{2\}$ in Eq. 8 instead of the average of $v_2\{2\}$ and $v_2\{4\}$. All individual sources are then added in quadrature to get the total systematic uncertainty. We have excluded any systematic variation in the assumption of $\kappa_2 \approx \kappa_3$ for the reported values of f_{CME} .

The total, centrality-independent systematic uncertainty is indicated by the shaded box on the line at

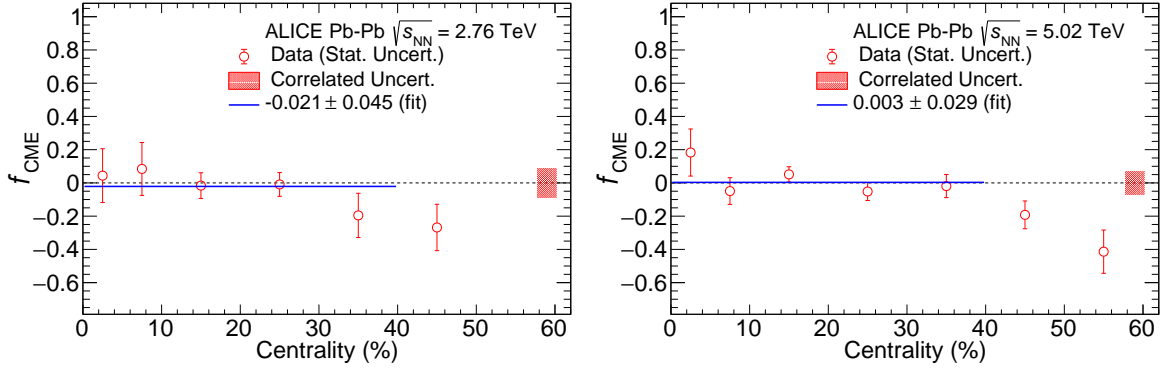


Figure 8: (Left panel) The CME fraction extracted in Pb–Pb collisions at $\sqrt{s_{\text{NN}}} = 2.76$ TeV. (Right panel) The CME fraction extracted in Pb–Pb collisions at $\sqrt{s_{\text{NN}}} = 5.02$ TeV. The systematic uncertainty is shown as hatched band at zero line around the centrality value of 60%. The solid blue lines correspond to fit with a constant function to the data points. See text for details.

zero. It is seen that for both energies f_{CME} is compatible with zero up to centrality $\approx 40\%$. For more peripheral collisions, the value of f_{CME} is negative. This could indicate that the background may not be the same in $\gamma_{1,2}$ as in $\gamma_{1,1}$ or that the background correlations may not have a linear dependence with centrality.

Finally, to estimate an upper limit on the contribution of the CME signal to the measurement of $\gamma_{1,1}$, the data points of f_{CME} are fitted with a constant function up to the 40% centrality interval. The fit yields values -0.021 ± 0.045 and 0.003 ± 0.029 in Pb–Pb collisions at $\sqrt{s_{\text{NN}}} = 2.76$ and 5.02 TeV, respectively. These results are consistent with zero CME fraction and correspond to upper limits on f_{CME} of 15–18% (20–24%) at 95% (99.7%) confidence level for the 0–40% centrality interval. The latter values are estimated assuming Gaussian distributed uncertainties and taking into account that the CME fraction has a lower bound of 0 (see Fig. 8).

6 Summary

In this article, we reported charge-dependent results for various two-particle correlators as well as two-particle correlations relative to different order symmetry planes. These measurements are extracted from the analysis of Pb–Pb collisions recorded by ALICE at $\sqrt{s_{\text{NN}}} = 2.76$ and 5.02 TeV. These correlators exhibit different sensitivity to the signal induced by the CME and to background effects, dominated by local charge conservations coupled to anisotropic flow.

All two-particle correlations of the form δ_m for $m = 1, 2, 3$ and 4 are dominated by background effects and exhibit a significant centrality dependence. Among them, only δ_1 exhibits a notable charge-dependent difference, which does not change significantly as a function of Δp_T , but increases with increasing \bar{p}_T and decreases with increasing $\Delta\eta$ of the pair. For higher harmonics, on the other hand, the charge-dependent differences become progressively smaller and are compatible with zero for δ_3 and δ_4 .

The CME sensitive two-particle correlations relative to the second order symmetry plane, $\gamma_{1,1}$ and $\gamma_{1,-3}$, exhibit a significant charge-dependent difference, which increases towards peripheral centrality intervals. Results on particle correlations relative to the third order symmetry plane, expressed by $\gamma_{1,2}$, that probe background effects associated with local charge conservation modulated by triangular flow (v_3), also show a significant charge-dependent difference, which increases for more peripheral events. Finally, correlations between two particles relative to the fourth order symmetry plane, that also have the potential to probe mainly background effects, show no significant difference for pairs with same and opposite

electric charges, however they are suffering from large statistical and systematic uncertainties.

A blast wave parametrisation that incorporates local charge conservation tuned to reproduce the components of the background, is not able to fully describe the magnitude of the charge-dependent differences of the CME-sensitive correlator $\gamma_{1,1}$. Finally, the results of correlations relative to Ψ_3 and Ψ_4 that probe mainly, if not solely, the contribution of the background clearly show that these background effects are the dominating factor to the measurements of $\gamma_{1,1}$.

Acknowledgements

The ALICE Collaboration would like to thank all its engineers and technicians for their invaluable contributions to the construction of the experiment and the CERN accelerator teams for the outstanding performance of the LHC complex. The ALICE Collaboration gratefully acknowledges the resources and support provided by all Grid centres and the Worldwide LHC Computing Grid (WLCG) collaboration. The ALICE Collaboration acknowledges the following funding agencies for their support in building and running the ALICE detector: A. I. Alikhanyan National Science Laboratory (Yerevan Physics Institute) Foundation (ANSL), State Committee of Science and World Federation of Scientists (WFS), Armenia; Austrian Academy of Sciences, Austrian Science Fund (FWF): [M 2467-N36] and Nationalstiftung für Forschung, Technologie und Entwicklung, Austria; Ministry of Communications and High Technologies, National Nuclear Research Center, Azerbaijan; Conselho Nacional de Desenvolvimento Científico e Tecnológico (CNPq), Financiadora de Estudos e Projetos (Finep), Fundação de Amparo à Pesquisa do Estado de São Paulo (FAPESP) and Universidade Federal do Rio Grande do Sul (UFRGS), Brazil; Ministry of Education of China (MOEC), Ministry of Science & Technology of China (MSTC) and National Natural Science Foundation of China (NSFC), China; Ministry of Science and Education and Croatian Science Foundation, Croatia; Centro de Aplicaciones Tecnológicas y Desarrollo Nuclear (CEADEN), Cubaenergía, Cuba; Ministry of Education, Youth and Sports of the Czech Republic, Czech Republic; The Danish Council for Independent Research | Natural Sciences, the VILLUM FONDEN and Danish National Research Foundation (DNRF), Denmark; Helsinki Institute of Physics (HIP), Finland; Commissariat à l’Energie Atomique (CEA) and Institut National de Physique Nucléaire et de Physique des Particules (IN2P3) and Centre National de la Recherche Scientifique (CNRS), France; Bundesministerium für Bildung und Forschung (BMBF) and GSI Helmholtzzentrum für Schwerionenforschung GmbH, Germany; General Secretariat for Research and Technology, Ministry of Education, Research and Religions, Greece; National Research, Development and Innovation Office, Hungary; Department of Atomic Energy Government of India (DAE), Department of Science and Technology, Government of India (DST), University Grants Commission, Government of India (UGC) and Council of Scientific and Industrial Research (CSIR), India; Indonesian Institute of Science, Indonesia; Centro Fermi - Museo Storico della Fisica e Centro Studi e Ricerche Enrico Fermi and Istituto Nazionale di Fisica Nucleare (INFN), Italy; Institute for Innovative Science and Technology, Nagasaki Institute of Applied Science (IIST), Japanese Ministry of Education, Culture, Sports, Science and Technology (MEXT) and Japan Society for the Promotion of Science (JSPS) KAKENHI, Japan; Consejo Nacional de Ciencia (CONACYT) y Tecnología, through Fondo de Cooperación Internacional en Ciencia y Tecnología (FONCICYT) and Dirección General de Asuntos del Personal Académico (DGAPA), Mexico; Nederlandse Organisatie voor Wetenschappelijk Onderzoek (NWO), Netherlands; The Research Council of Norway, Norway; Commission on Science and Technology for Sustainable Development in the South (COMSATS), Pakistan; Pontificia Universidad Católica del Perú, Peru; Ministry of Science and Higher Education, National Science Centre and WUT ID-UB, Poland; Korea Institute of Science and Technology Information and National Research Foundation of Korea (NRF), Republic of Korea; Ministry of Education and Scientific Research, Institute of Atomic Physics and Ministry of Research and Innovation and Institute of Atomic Physics, Romania; Joint Institute for Nuclear Research (JINR), Ministry of Education and Science of the Russian Federation, National Research Centre Kurchatov Institute, Russian Science Foundation and

Russian Foundation for Basic Research, Russia; Ministry of Education, Science, Research and Sport of the Slovak Republic, Slovakia; National Research Foundation of South Africa, South Africa; Swedish Research Council (VR) and Knut & Alice Wallenberg Foundation (KAW), Sweden; European Organization for Nuclear Research, Switzerland; Suranaree University of Technology (SUT), National Science and Technology Development Agency (NSDTA) and Office of the Higher Education Commission under NRU project of Thailand, Thailand; Turkish Atomic Energy Agency (TAEK), Turkey; National Academy of Sciences of Ukraine, Ukraine; Science and Technology Facilities Council (STFC), United Kingdom; National Science Foundation of the United States of America (NSF) and United States Department of Energy, Office of Nuclear Physics (DOE NP), United States of America.

References

- [1] E. V. Shuryak, “Theory and phenomenology of the QCD vacuum”, *Phys. Rept.* **115** (1984) 151.
- [2] J. Cleymans, R. V. Gavai, and E. Suhonen, “Quarks and Gluons at High Temperatures and Densities”, *Phys. Rept.* **130** (1986) 217.
- [3] S. A. Bass, M. Gyulassy, H. Stoecker, and W. Greiner, “Signatures of quark gluon plasma formation in high-energy heavy ion collisions: A Critical review”, *J. Phys.* **G25** (1999) R1–R57, arXiv:hep-ph/9810281 [hep-ph].
- [4] S. Borsanyi, G. Endrodi, Z. Fodor, A. Jakovac, S. D. Katz, S. Krieg, C. Ratti, and K. K. Szabo, “The QCD equation of state with dynamical quarks”, *JHEP* **11** (2010) 077, arXiv:1007.2580 [hep-lat].
- [5] T. Bhattacharya *et al.*, “QCD Phase Transition with Chiral Quarks and Physical Quark Masses”, *Phys. Rev. Lett.* **113** no. 8, (2014) 082001, arXiv:1402.5175 [hep-lat].
- [6] T. D. Lee, “A Theory of Spontaneous T Violation”, *Phys. Rev.* **D8** (1973) 1226–1239. [516(1973)].
- [7] T. D. Lee and G. C. Wick, “Vacuum Stability and Vacuum Excitation in a Spin 0 Field Theory”, *Phys. Rev.* **D9** (1974) 2291–2316.
- [8] A. Bzdak and V. Skokov, “Event-by-event fluctuations of magnetic and electric fields in heavy ion collisions”, *Phys. Lett.* **B710** (2012) 171–174, arXiv:1111.1949 [hep-ph].
- [9] P. D. Morley and I. A. Schmidt, “Strong P, CP, T Violations in Heavy Ion Collisions”, *Z. Phys.* **C26** (1985) 627.
- [10] D. Kharzeev, R. D. Pisarski, and M. H. G. Tytgat, “Possibility of spontaneous parity violation in hot QCD”, *Phys. Rev. Lett.* **81** (1998) 512–515, arXiv:hep-ph/9804221 [hep-ph].
- [11] D. Kharzeev and R. D. Pisarski, “Pionic measures of parity and CP violation in high-energy nuclear collisions”, *Phys. Rev.* **D61** (2000) 111901, arXiv:hep-ph/9906401 [hep-ph].
- [12] D. E. Kharzeev, “The Chiral Magnetic Effect and Anomaly-Induced Transport”, *Prog. Part. Nucl. Phys.* **75** (2014) 133–151, arXiv:1312.3348 [hep-ph].
- [13] D. E. Kharzeev, “Topology, magnetic field, and strongly interacting matter”, *Ann. Rev. Nucl. Part. Sci.* **65** (2015) 193–214, arXiv:1501.01336 [hep-ph].
- [14] D. Kharzeev and A. Zhitnitsky, “Charge separation induced by P-odd bubbles in QCD matter”, *Nucl. Phys.* **A797** (2007) 67–79, arXiv:0706.1026 [hep-ph].

- [15] K. Fukushima, D. E. Kharzeev, and H. J. Warringa, “The Chiral Magnetic Effect”, *Phys. Rev.* **D78** (2008) 074033, arXiv:0808.3382 [hep-ph].
- [16] D. E. Kharzeev, L. D. McLerran, and H. J. Warringa, “The Effects of topological charge change in heavy ion collisions: ‘Event by event P and CP violation’”, *Nucl. Phys.* **A803** (2008) 227–253, arXiv:0711.0950 [hep-ph].
- [17] Q. Li, D. E. Kharzeev, C. Zhang, Y. Huang, I. Pletikosic, A. V. Fedorov, R. D. Zhong, J. A. Schneeloch, G. D. Gu, and T. Valla, “Observation of the chiral magnetic effect in ZrTe5”, *Nature Phys.* **12** (2016) 550–554, arXiv:1412.6543 [cond-mat.str-el].
- [18] S. Voloshin and Y. Zhang, “Flow study in relativistic nuclear collisions by Fourier expansion of Azimuthal particle distributions”, *Z. Phys.* **C70** (1996) 665–672, arXiv:hep-ph/9407282 [hep-ph].
- [19] **PHOBOS** Collaboration, S. Manly *et al.*, “System size, energy and pseudorapidity dependence of directed and elliptic flow at RHIC”, *Nucl. Phys.* **A774** (2006) 523–526, arXiv:nucl-ex/0510031 [nucl-ex].
- [20] R. S. Bhalerao and J.-Y. Ollitrault, “Eccentricity fluctuations and elliptic flow at RHIC”, *Phys. Lett.* **B641** (2006) 260–264, arXiv:nucl-th/0607009 [nucl-th].
- [21] B. Alver *et al.*, “Importance of correlations and fluctuations on the initial source eccentricity in high-energy nucleus-nucleus collisions”, *Phys. Rev.* **C77** (2008) 014906, arXiv:0711.3724 [nucl-ex].
- [22] B. Alver and G. Roland, “Collision geometry fluctuations and triangular flow in heavy-ion collisions”, *Phys. Rev.* **C81** (2010) 054905, arXiv:1003.0194 [nucl-th]. [Erratum: *Phys. Rev.* C82,039903(2010)].
- [23] B. H. Alver, C. Gombeaud, M. Luzum, and J.-Y. Ollitrault, “Triangular flow in hydrodynamics and transport theory”, *Phys. Rev.* **C82** (2010) 034913, arXiv:1007.5469 [nucl-th].
- [24] S. A. Voloshin, “Parity violation in hot QCD: How to detect it”, *Phys. Rev.* **C70** (2004) 057901, arXiv:hep-ph/0406311 [hep-ph].
- [25] **ALICE** Collaboration, B. Abelev *et al.*, “Charge separation relative to the reaction plane in Pb-Pb collisions at $\sqrt{s_{NN}} = 2.76$ TeV”, *Phys. Rev. Lett.* **110** no. 1, (2013) 012301, arXiv:1207.0900 [nucl-ex].
- [26] **STAR** Collaboration, B. I. Abelev *et al.*, “Azimuthal Charged-Particle Correlations and Possible Local Strong Parity Violation”, *Phys. Rev. Lett.* **103** (2009) 251601, arXiv:0909.1739 [nucl-ex].
- [27] **STAR** Collaboration, B. I. Abelev *et al.*, “Observation of charge-dependent azimuthal correlations and possible local strong parity violation in heavy ion collisions”, *Phys. Rev.* **C81** (2010) 054908, arXiv:0909.1717 [nucl-ex].
- [28] **STAR** Collaboration, L. Adamczyk *et al.*, “Measurement of charge multiplicity asymmetry correlations in high-energy nucleus-nucleus collisions at $\sqrt{s_{NN}} = 200$ GeV”, *Phys. Rev.* **C89** no. 4, (2014) 044908, arXiv:1303.0901 [nucl-ex].
- [29] **STAR** Collaboration, L. Adamczyk *et al.*, “Fluctuations of charge separation perpendicular to the event plane and local parity violation in $\sqrt{s_{NN}} = 200$ GeV Au+Au collisions at the BNL Relativistic Heavy Ion Collider”, *Phys. Rev.* **C88** no. 6, (2013) 064911, arXiv:1302.3802 [nucl-ex].

- [30] **STAR** Collaboration, L. Adamczyk *et al.*, “Beam-energy dependence of charge separation along the magnetic field in Au+Au collisions at RHIC”, *Phys. Rev. Lett.* **113** (2014) 052302, arXiv:1404.1433 [nucl-ex].
- [31] S. Schlichting and S. Pratt, “Charge conservation at energies available at the BNL Relativistic Heavy Ion Collider and contributions to local parity violation observables”, *Phys. Rev.* **C83** (2011) 014913, arXiv:1009.4283 [nucl-th].
- [32] S. Pratt, S. Schlichting, and S. Gavin, “Effects of Momentum Conservation and Flow on Angular Correlations at RHIC”, *Phys. Rev.* **C84** (2011) 024909, arXiv:1011.6053 [nucl-th].
- [33] **ALICE** Collaboration, S. Acharya *et al.*, “Constraining the magnitude of the Chiral Magnetic Effect with Event Shape Engineering in Pb-Pb collisions at $\sqrt{s_{NN}} = 2.76$ TeV”, *Phys. Lett.* **B777** (2018) 151–162, arXiv:1709.04723 [nucl-ex].
- [34] J. Schukraft, A. Timmins, and S. A. Voloshin, “Ultra-relativistic nuclear collisions: event shape engineering”, *Phys. Lett.* **B719** (2013) 394–398, arXiv:1208.4563 [nucl-ex].
- [35] **CMS** Collaboration, V. Khachatryan *et al.*, “Observation of charge-dependent azimuthal correlations in p -Pb collisions and its implication for the search for the chiral magnetic effect”, *Phys. Rev. Lett.* **118** no. 12, (2017) 122301, arXiv:1610.00263 [nucl-ex].
- [36] **STAR** Collaboration, J. Adam *et al.*, “Charge-dependent pair correlations relative to a third particle in $p + Au$ and $d + Au$ collisions at RHIC”, *Phys. Lett.* **B798** (2019) 134975, arXiv:1906.03373 [nucl-ex].
- [37] **ATLAS** Collaboration, G. Aad *et al.*, “Measurement of event-plane correlations in $\sqrt{s_{NN}} = 2.76$ TeV lead-lead collisions with the ATLAS detector”, *Phys. Rev.* **C90** no. 2, (2014) 024905, arXiv:1403.0489 [hep-ex].
- [38] **CMS** Collaboration, A. M. Sirunyan *et al.*, “Constraints on the chiral magnetic effect using charge-dependent azimuthal correlations in pPb and $PbPb$ collisions at the CERN Large Hadron Collider”, *Phys. Rev.* **C97** no. 4, (2018) 044912, arXiv:1708.01602 [nucl-ex].
- [39] S. A. Voloshin, “Collective phenomena in ultra-relativistic nuclear collisions: anisotropic flow and more”, *Prog. Part. Nucl. Phys.* **67** (2012) 541–546, arXiv:1111.7241 [nucl-ex].
- [40] **ALICE** Collaboration, K. Aamodt *et al.*, “The ALICE experiment at the CERN LHC”, *JINST* **3** (2008) S08002.
- [41] J. Alme *et al.*, “The ALICE TPC, a large 3-dimensional tracking device with fast readout for ultra-high multiplicity events”, *Nucl. Instrum. Meth.* **A622** (2010) 316–367, arXiv:1001.1950 [physics.ins-det].
- [42] **ALICE** Collaboration, E. Abbas *et al.*, “Performance of the ALICE VZERO system”, *JINST* **8** (2013) P10016, arXiv:1306.3130 [nucl-ex].
- [43] **ALICE** Collaboration, B. B. Abelev *et al.*, “Performance of the ALICE Experiment at the CERN LHC”, *Int. J. Mod. Phys.* **A29** (2014) 1430044, arXiv:1402.4476 [nucl-ex].
- [44] **ALICE** Collaboration, B. Abelev *et al.*, “Centrality determination of Pb-Pb collisions at $\sqrt{s_{NN}} = 2.76$ TeV with ALICE”, *Phys. Rev.* **C88** no. 4, (2013) 044909, arXiv:1301.4361 [nucl-ex].
- [45] P. Billoir, “Track Fitting With Multiple Scattering: A New Method”, *Nucl. Instrum. Meth.* **A225** (1984) 352–366.

- [46] P. Billoir, R. Fruhwirth, and M. Regler, “Track element merging strategy and vertex fitting in complex modular detectors”, *Nucl. Instrum. Meth.* **A241** (1985) 115–131.
- [47] U. Gursoy, D. Kharzeev, E. Marcus, K. Rajagopal, and C. Shen, “Charge-dependent Flow Induced by Magnetic and Electric Fields in Heavy Ion Collisions”, *Phys. Rev.* **C98** no. 5, (2018) 055201, arXiv:1806.05288 [hep-ph].
- [48] A. Bzdak, V. Koch, and J. Liao, “Charge-Dependent Correlations in Relativistic Heavy Ion Collisions and the Chiral Magnetic Effect”, *Lect. Notes Phys.* **871** (2013) 503–536, arXiv:1207.7327 [nucl-th].
- [49] F. Retiere and M. A. Lisa, “Observable implications of geometrical and dynamical aspects of freeze out in heavy ion collisions”, *Phys. Rev.* **C70** (2004) 044907, arXiv:nucl-th/0312024 [nucl-th].
- [50] B. Zhang, C. M. Ko, B.-A. Li, and Z.-W. Lin, “A multiphase transport model for nuclear collisions at RHIC”, *Phys. Rev.* **C61** (2000) 067901, arXiv:nucl-th/9907017 [nucl-th].
- [51] Z.-W. Lin, S. Pal, C. M. Ko, B.-A. Li, and B. Zhang, “Charged particle rapidity distributions at relativistic energies”, *Phys. Rev.* **C64** (2001) 011902, arXiv:nucl-th/0011059 [nucl-th].
- [52] Z.-W. Lin, C. M. Ko, B.-A. Li, B. Zhang, and S. Pal, “A Multi-phase transport model for relativistic heavy ion collisions”, *Phys. Rev.* **C72** (2005) 064901, arXiv:nucl-th/0411110 [nucl-th].
- [53] A. M. Poskanzer and S. A. Voloshin, “Methods for analyzing anisotropic flow in relativistic nuclear collisions”, *Phys. Rev.* **C58** (1998) 1671–1678, arXiv:nucl-ex/9805001 [nucl-ex].
- [54] S. A. Voloshin, A. M. Poskanzer, and R. Snellings, “Collective phenomena in non-central nuclear collisions”, *Landolt-Bornstein* **23** (2010) 293–333, arXiv:0809.2949 [nucl-ex].
- [55] R. Barlow, “Systematic errors: Facts and fictions”, in *Advanced Statistical Techniques in Particle Physics. Proceedings, Conference, Durham, UK, March 18-22, 2002*, pp. 134–144. 2002. arXiv:hep-ex/0207026 [hep-ex].
- [56] ALICE Collaboration, B. Abelev *et al.*, “Charge correlations using the balance function in Pb–Pb collisions at $\sqrt{s_{NN}} = 2.76$ TeV”, *Phys. Lett.* **B723** (2013) 267–279, arXiv:1301.3756 [nucl-ex].
- [57] ALICE Collaboration, J. Adam *et al.*, “Multiplicity and transverse momentum evolution of charge-dependent correlations in pp, p–Pb, and Pb–Pb collisions at the LHC”, *Eur. Phys. J.* **C76** no. 2, (2016) 86, arXiv:1509.07255 [nucl-ex].
- [58] ALICE Collaboration, S. Acharya *et al.*, “Energy dependence and fluctuations of anisotropic flow in Pb-Pb collisions at $\sqrt{s_{NN}} = 5.02$ and 2.76 TeV”, *JHEP* **07** (2018) 103, arXiv:1804.02944 [nucl-ex].
- [59] ALICE Collaboration, S. Acharya *et al.*, “Production of charged pions, kaons and (anti-)protons in Pb-Pb and inelastic pp collisions at $\sqrt{s_{NN}} = 5.02$ TeV”, arXiv:1910.07678 [nucl-ex].
- [60] ALICE Collaboration, S. Acharya *et al.*, “Anisotropic flow of identified particles in Pb-Pb collisions at $\sqrt{s_{NN}} = 5.02$ TeV”, *JHEP* **09** (2018) 006, arXiv:1805.04390 [nucl-ex].
- [61] B. Zhang, “ZPC 1.0.1: A Parton cascade for ultrarelativistic heavy ion collisions”, *Comput. Phys. Commun.* **109** (1998) 193–206, arXiv:nucl-th/9709009 [nucl-th].

- [62] **ALICE** Collaboration, K. Aamodt *et al.*, “Elliptic flow of charged particles in Pb-Pb collisions at 2.76 TeV”, *Phys. Rev. Lett.* **105** (2010) 252302, arXiv:1011.3914 [nucl-ex].
- [63] S. Choudhury, G. Wang, W. He, Y. Hu, and H. Z. Huang, “Background evaluations for the chiral magnetic effect with normalized correlators using a multiphase transport model”, arXiv:1909.04083 [hep-ph].
- [64] S. A. Voloshin, A. M. Poskanzer, A. Tang, and G. Wang, “Elliptic flow in the Gaussian model of eccentricity fluctuations”, *Phys. Lett. B* **659** (2008) 537–541, arXiv:0708.0800 [nucl-th].

A The ALICE Collaboration

S. Acharya¹⁴¹, D. Adamová⁹⁵, A. Adler⁷⁴, J. Adolfsson⁸¹, M.M. Aggarwal¹⁰⁰, G. Aglieri Rinella³⁴, M. Agnello³⁰, N. Agrawal^{10,54}, Z. Ahmed¹⁴¹, S. Ahmad¹⁶, S.U. Ahn⁷⁶, Z. Akbar⁵¹, A. Akindinov⁹², M. Al-Turany¹⁰⁷, S.N. Alam^{40,141}, D.S.D. Albuquerque¹²², D. Aleksandrov⁸⁸, B. Alessandro⁵⁹, H.M. Alfanda⁶, R. Alfaro Molina⁷¹, B. Ali¹⁶, Y. Ali¹⁴, A. Alici^{10,26,54}, A. Alkin^{2,34}, J. Alme²¹, T. Alt⁶⁸, L. Altenkamper²¹, I. Altsybeev¹¹³, M.N. Anaam⁶, C. Andrei⁴⁸, D. Andreou³⁴, A. Andronic¹⁴⁴, M. Angeletti³⁴, V. Anguelov¹⁰⁴, C. Anson¹⁵, T. Antičić¹⁰⁸, F. Antinori⁵⁷, P. Antonioli⁵⁴, N. Apadula⁸⁰, L. Aphecetche¹¹⁵, H. Appelshäuser⁶⁸, S. Arcelli²⁶, R. Arnaldi⁵⁹, M. Arratia⁸⁰, I.C. Arsene²⁰, M. Arslanok¹⁰⁴, A. Augustinus³⁴, R. Averbeck¹⁰⁷, S. Aziz⁷⁸, M.D. Azmi¹⁶, A. Badalà⁵⁶, Y.W. Baek⁴¹, S. Bagnasco⁵⁹, X. Bai¹⁰⁷, R. Bailhache⁶⁸, R. Bala¹⁰¹, A. Balbino³⁰, A. Baldisseri¹³⁷, M. Ball⁴³, S. Balouza¹⁰⁵, D. Banerjee³, R. Barbera²⁷, L. Barioglio²⁵, G.G. Barnaföldi¹⁴⁵, L.S. Barnby⁹⁴, V. Barret¹³⁴, P. Bartalini⁶, C. Bartels¹²⁷, K. Barth³⁴, E. Bartsch⁶⁸, F. Baruffaldi²⁸, N. Bastid¹³⁴, S. Basu¹⁴³, G. Batigne¹¹⁵, B. Batyunya⁷⁵, D. Bauri⁴⁹, J.L. Bazo Alba¹¹², I.G. Bearden⁸⁹, C. Beattie¹⁴⁶, C. Bedda⁶³, N.K. Behera⁶¹, I. Belikov¹³⁶, A.D.C. Bell Hechavarria¹⁴⁴, F. Bellini³⁴, R. Bellwied¹²⁵, V. Belyaev⁹³, G. Bencedi¹⁴⁵, S. Beole²⁵, A. Bercuci⁴⁸, Y. Berdnikov⁹⁸, D. Berenyi¹⁴⁵, R.A. Bertens¹³⁰, D. Berzano⁵⁹, M.G. Besoiu⁶⁷, L. Betev³⁴, A. Bhasin¹⁰¹, I.R. Bhat¹⁰¹, M.A. Bhat³, H. Bhatt⁴⁹, B. Bhattacharjee⁴², A. Bianchi²⁵, L. Bianchi²⁵, N. Bianchi⁵², J. Bielčik³⁷, J. Bielčiková⁹⁵, A. Bilandzic¹⁰⁵, G. Biro¹⁴⁵, R. Biswas³, S. Biswas³, J.T. Blair¹¹⁹, D. Blau⁸⁸, C. Blume⁶⁸, G. Boca¹³⁹, F. Bock⁹⁶, A. Bogdanov⁹³, S. Boi²³, J. Bok⁶¹, L. Boldizsár¹⁴⁵, A. Bolozdynya⁹³, M. Bombara³⁸, G. Bonomi¹⁴⁰, H. Borel¹³⁷, A. Borissov⁹³, H. Bossi¹⁴⁶, E. Botta²⁵, L. Bratrud⁶⁸, P. Braun-Munzinger¹⁰⁷, M. Bregant¹²¹, M. Broz³⁷, E. Bruna⁵⁹, G.E. Bruno¹⁰⁶, M.D. Buckland¹²⁷, D. Budnikov¹⁰⁹, H. Buesching⁶⁸, S. Bufalino³⁰, O. Bugnon¹¹⁵, P. Buhler¹¹⁴, P. Buncic³⁴, Z. Buthelezi^{72,131}, J.B. Butt¹⁴, S.A. Bysiak¹¹⁸, D. Caffarri⁹⁰, A. Caliva¹⁰⁷, E. Calvo Villar¹¹², R.S. Camacho⁴⁵, P. Camerini²⁴, A.A. Capon¹¹⁴, F. Carnesecchi²⁶, R. Caron¹³⁷, J. Castillo Castellanos¹³⁷, A.J. Castro¹³⁰, E.A.R. Casula⁵⁵, F. Catalano³⁰, C. Ceballos Sanchez⁵³, P. Chakraborty⁴⁹, S. Chandra¹⁴¹, W. Chang⁶, S. Chapeland³⁴, M. Chartier¹²⁷, S. Chattopadhyay¹⁴¹, S. Chattopadhyay¹¹⁰, A. Chauvin²³, C. Cheshkov¹³⁵, B. Cheynis¹³⁵, V. Chibante Barroso³⁴, D.D. Chinellato¹²², S. Cho⁶¹, P. Chochula³⁴, T. Chowdhury¹³⁴, P. Christakoglou⁹⁰, C.H. Christensen⁸⁹, P. Christiansen⁸¹, T. Chujo¹³³, C. Cicalo⁵⁵, L. Cifarelli^{10,26}, F. Cindolo⁵⁴, G. Clai^{54,ii}, J. Cleymans¹²⁴, F. Colamaria⁵³, D. Colella⁵³, A. Collu⁸⁰, M. Colocci²⁶, M. Concas^{59,iii}, G. Conesa Balbastre⁷⁹, Z. Conesa del Valle⁷⁸, G. Contin^{24,60}, J.G. Contreras³⁷, T.M. Cormier⁹⁶, Y. Corrales Morales²⁵, P. Cortese³¹, M.R. Cosentino¹²³, F. Costa³⁴, S. Costanza¹³⁹, P. Crochet¹³⁴, E. Cuautle⁶⁹, P. Cui⁶, L. Cunqueiro⁹⁶, D. Dabrowski¹⁴², T. Dahms¹⁰⁵, A. Dainese⁵⁷, F.P.A. Damas^{115,137}, M.C. Danisch¹⁰⁴, A. Danu⁶⁷, D. Das¹¹⁰, I. Das¹¹⁰, P. Das⁸⁶, P. Das³, S. Das³, A. Dash⁸⁶, N. Dash⁴⁹, S. De⁸⁶, A. De Caro²⁹, G. de Cataldo⁵³, J. de Cuveland³⁹, A. De Falco²³, D. De Gruttola¹⁰, N. De Marco⁵⁹, S. De Pasquale²⁹, S. Deb⁵⁰, H.F. Degenhardt¹²¹, K.R. Deja¹⁴², A. Deloff⁸⁵, S. Delsanto^{25,131}, W. Deng⁶, P. Dhankher⁴⁹, D. Di Bari³³, A. Di Mauro³⁴, R.A. Diaz⁸, T. Dietel¹²⁴, P. Dillenseger⁶⁸, Y. Ding⁶, R. Diviã³⁴, D.U. Dixit¹⁹, Ø. Djuvsland²¹, U. Dmitrieva⁶², A. Dobrin⁶⁷, B. Dönigus⁶⁸, O. Dordic²⁰, A.K. Dubey¹⁴¹, A. Dubla^{90,107}, S. Dudi¹⁰⁰, M. Dukhishyam⁸⁶, P. Dupieux¹³⁴, R.J. Ehlers^{96,146}, V.N. Eikeland²¹, D. Elia⁵³, B. Erazmus¹¹⁵, F. Erhardt⁹⁹, A. Erokhin¹¹³, M.R. Ersdal²¹, B. Espagnon⁷⁸, G. Eulisse³⁴, D. Evans¹¹¹, S. Evdokimov⁹¹, L. Fabbietti¹⁰⁵, M. Faggin²⁸, J. Faivre⁷⁹, F. Fan⁶, A. Fantoni⁵², M. Fasel⁹⁶, P. Fecchio³⁰, A. Feliciello⁵⁹, G. Feofilov¹¹³, A. Fernández Téllez⁴⁵, A. Ferrero¹³⁷, A. Ferretti²⁵, A. Festanti³⁴, V.J.G. Feuillard¹⁰⁴, J. Figiel¹¹⁸, S. Filchagin¹⁰⁹, D. Finogeev⁶², F.M. Fionda²¹, G. Fiorenza⁵³, F. Flor¹²⁵, A.N. Flores¹¹⁹, S. Foertsch⁷², P. Foka¹⁰⁷, S. Fokin⁸⁸, E. Fragiacomo⁶⁰, U. Frankenfeld¹⁰⁷, U. Fuchs³⁴, C. Furget⁷⁹, A. Furs⁶², M. Fusco Girard²⁹, J.J. Gaardhøje⁸⁹, M. Gagliardi²⁵, A.M. Gago¹¹², A. Gal¹³⁶, C.D. Galvan¹²⁰, P. Ganoti⁸⁴, C. Garabatos¹⁰⁷, J.R.A. Garcia⁴⁵, E. Garcia-Solis¹¹, K. Garg¹¹⁵, C. Gargiulo³⁴, A. Garibli⁸⁷, K. Garner¹⁴⁴, P. Gasik^{105,107}, E.F. Gauger¹¹⁹, M.B. Gay Ducati⁷⁰, M. Germain¹¹⁵, J. Ghosh¹¹⁰, P. Ghosh¹⁴¹, S.K. Ghosh³, M. Giacalone²⁶, P. Gianotti⁵², P. Giubellino^{59,107}, P. Giubilato²⁸, P. Glässel¹⁰⁴, A. Gomez Ramirez⁷⁴, V. Gonzalez^{107,143}, L.H. González-Trueba⁷¹, S. Gorbunov³⁹, L. Görlich¹¹⁸, A. Goswami⁴⁹, S. Gotovac³⁵, V. Grabski⁷¹, L.K. Graczykowski¹⁴², K.L. Graham¹¹¹, L. Greiner⁸⁰, A. Grelli⁶³, C. Grigoras³⁴, V. Grigoriev⁹³, A. Grigoryan¹, S. Grigoryan⁷⁵, O.S. Groettvik²¹, F. Grosa^{30,59}, J.F. Grosse-Oetringhaus³⁴, R. Grosso¹⁰⁷, R. Guernane⁷⁹, M. Guittiere¹¹⁵, K. Gulbrandsen⁸⁹, T. Gunji¹³², A. Gupta¹⁰¹, R. Gupta¹⁰¹, I.B. Guzman⁴⁵, R. Haake¹⁴⁶, M.K. Habib¹⁰⁷, C. Hadjidakis⁷⁸, H. Hamagaki⁸², G. Hamar¹⁴⁵, M. Hamid⁶, R. Hannigan¹¹⁹, M.R. Haque^{63,86}, A. Harlanderova¹⁰⁷, J.W. Harris¹⁴⁶, A. Harton¹¹, J.A. Hasenbichler³⁴, H. Hassan⁹⁶, Q.U. Hassan¹⁴, D. Hatzifotiadou^{10,54}, P. Hauer⁴³, L.B. Havener¹⁴⁶, S. Hayashi¹³², S.T. Heckel¹⁰⁵, E. Hellbär⁶⁸, H. Helstrup³⁶, A. Herghelegiu⁴⁸, T. Herman³⁷, E.G. Hernandez⁴⁵, G. Herrera Corral⁹, F. Herrmann¹⁴⁴, K.F. Hetland³⁶, H. Hillemanns³⁴, C. Hills¹²⁷, B. Hippolyte¹³⁶, B. Hohlweger¹⁰⁵, J. Honermann¹⁴⁴,

D. Horak³⁷, A. Hornung⁶⁸, S. Hornung¹⁰⁷, R. Hosokawa¹⁵, P. Hristov³⁴, C. Huang⁷⁸, C. Hughes¹³⁰, P. Huhn⁶⁸, T.J. Humanic⁹⁷, H. Hushnud¹¹⁰, L.A. Husova¹⁴⁴, N. Hussain⁴², S.A. Hussain¹⁴, D. Hutter³⁹, J.P. Iddon^{34,127}, R. Ilkaev¹⁰⁹, H. Ilyas¹⁴, M. Inaba¹³³, G.M. Innocenti³⁴, M. Ippolitov⁸⁸, A. Isakov⁹⁵, M.S. Islam¹¹⁰, M. Ivanov¹⁰⁷, V. Ivanov⁹⁸, V. Izucheev⁹¹, B. Jacak⁸⁰, N. Jacazio^{34,54}, P.M. Jacobs⁸⁰, S. Jadlovská¹¹⁷, J. Jádlovský¹¹⁷, S. Jaelani⁶³, C. Jahnke¹²¹, M.J. Jakubowska¹⁴², M.A. Janik¹⁴², T. Janson⁷⁴, M. Jercic⁹⁹, O. Jevons¹¹¹, M. Jin¹²⁵, F. Jonas^{96,144}, P.G. Jones¹¹¹, J. Jung⁶⁸, M. Jung⁶⁸, A. Jusko¹¹¹, P. Kalinák⁶⁴, A. Kalweit³⁴, V. Kaplin⁹³, S. Kar⁶, A. Karasu Uysal⁷⁷, O. Karavichev⁶², T. Karavicheva⁶², P. Karczmarczyk³⁴, E. Karpechev⁶², A. Kazantsev⁸⁸, U. Kebschull⁷⁴, R. Keidel⁴⁷, M. Keil³⁴, B. Ketzer⁴³, Z. Khabanova⁹⁰, A.M. Khan⁶, S. Khan¹⁶, S.A. Khan¹⁴¹, A. Khanzadeev⁹⁸, Y. Kharlov⁹¹, A. Khatun¹⁶, A. Khuntia¹¹⁸, B. Kileng³⁶, B. Kim⁶¹, B. Kim¹³³, D. Kim¹⁴⁷, D.J. Kim¹²⁶, E.J. Kim⁷³, H. Kim¹⁷, J. Kim¹⁴⁷, J.S. Kim⁴¹, J. Kim¹⁰⁴, J. Kim¹⁴⁷, J. Kim⁷³, M. Kim¹⁰⁴, S. Kim¹⁸, T. Kim¹⁴⁷, T. Kim¹⁴⁷, S. Kirsch⁶⁸, I. Kisel³⁹, S. Kiselev⁹², A. Kisiel¹⁴², J.L. Klay⁵, C. Klein⁶⁸, J. Klein^{34,59}, S. Klein⁸⁰, C. Klein-Bösing¹⁴⁴, M. Kleiner⁶⁸, A. Kluge³⁴, M.L. Knichel³⁴, A.G. Knospe¹²⁵, C. Kobdaj¹¹⁶, M.K. Köhler¹⁰⁴, T. Kollegger¹⁰⁷, A. Kondratyev⁷⁵, N. Kondratyeva⁹³, E. Kondratyuk⁹¹, J. König⁶⁸, S.A. Königstorfer¹⁰⁵, P.J. Konopka³⁴, G. Kornakov¹⁴², L. Koska¹¹⁷, O. Kovalenko⁸⁵, V. Kovalenko¹¹³, M. Kowalski¹¹⁸, I. Králik⁶⁴, A. Kravčáková³⁸, L. Kreis¹⁰⁷, M. Krivda^{64,111}, F. Krizek⁹⁵, K. Krizkova Gajdosova³⁷, M. Krüger⁶⁸, E. Kryshen⁹⁸, M. Krzewicki³⁹, A.M. Kubera⁹⁷, V. Kučera^{34,61}, C. Kuhn¹³⁶, P.G. Kuijter⁹⁰, L. Kumar¹⁰⁰, S. Kundu⁸⁶, P. Kurashvili⁸⁵, A. Kurepin⁶², A.B. Kurepin⁶², A. Kuryakin¹⁰⁹, S. Kushpil⁹⁵, J. Kvapil¹¹¹, M.J. Kwon⁶¹, J.Y. Kwon⁶¹, Y. Kwon¹⁴⁷, S.L. La Pointe³⁹, P. La Rocca²⁷, Y.S. Lai⁸⁰, M. Lamanna³⁴, R. Langoy¹²⁹, K. Lapidus³⁴, A. Lardeux²⁰, P. Larionov⁵², E. Laudi³⁴, R. Lavicka³⁷, T. Lazareva¹¹³, R. Lea²⁴, L. Leardini¹⁰⁴, J. Lee¹³³, S. Lee¹⁴⁷, F. Lehas⁹⁰, S. Lehner¹¹⁴, J. Lehrbach³⁹, R.C. Lemmon⁹⁴, I. León Monzón¹²⁰, E.D. Lesser¹⁹, M. Lettrich³⁴, P. Lévai¹⁴⁵, X. Li¹², X.L. Li⁶, J. Lien¹²⁹, R. Lietava¹¹¹, B. Lim¹⁷, V. Lindenstruth³⁹, A. Lindner⁴⁸, C. Lippmann¹⁰⁷, M.A. Lisa⁹⁷, A. Liu¹⁹, J. Liu¹²⁷, S. Liu⁹⁷, W.J. Llope¹⁴³, I.M. Lofnes²¹, V. Loginov⁹³, C. Loizides⁹⁶, P. Loncar³⁵, J.A. Lopez¹⁰⁴, X. Lopez¹³⁴, E. López Torres⁸, J.R. Luhder¹⁴⁴, M. Lunardon²⁸, G. Luparello⁶⁰, Y.G. Ma⁴⁰, A. Maevskaya⁶², M. Mager³⁴, S.M. Mahmood²⁰, T. Mahmoud⁴³, A. Maire¹³⁶, R.D. Majka^{146,ii}, M. Malaev⁹⁸, Q.W. Malik²⁰, L. Malinina^{75,iv}, D. Mal'Kevich⁹², P. Malzacher¹⁰⁷, G. Mandaglio^{32,56}, V. Manko⁸⁸, F. Manso¹³⁴, V. Manzari⁵³, Y. Mao⁶, M. Marchisone¹³⁵, J. Mareš⁶⁶, G.V. Margagliotti²⁴, A. Margotti⁵⁴, J. Margutti⁶³, A. Marín¹⁰⁷, C. Markert¹¹⁹, M. Marquard⁶⁸, C.D. Martin²⁴, N.A. Martin¹⁰⁴, P. Martinengo³⁴, J.L. Martinez¹²⁵, M.I. Martínez⁴⁵, G. Martínez García¹¹⁵, S. Masciocchi¹⁰⁷, M. Masera²⁵, A. Masoni⁵⁵, L. Massacrier⁷⁸, E. Masson¹¹⁵, A. Mastroserio^{53,138}, A.M. Mathis¹⁰⁵, O. Matonoha⁸¹, P.F.T. Matuoka¹²¹, A. Matyja¹¹⁸, C. Mayer¹¹⁸, F. Mazzaschi²⁵, M. Mazzilli⁵³, M.A. Mazzoni⁵⁸, A.F. Mechler⁶⁸, F. Meddi²², Y. Melikyan^{62,93}, A. Menchaca-Rocha⁷¹, C. Mengke⁶, E. Meninno^{29,114}, M. Meres¹³, S. Mhlanga¹²⁴, Y. Miake¹³³, L. Micheletti²⁵, L.C. Migliorin¹³⁵, D.L. Mihaylov¹⁰⁵, K. Mikhaylov^{75,92}, A.N. Mishra⁶⁹, D. Miśkowiec¹⁰⁷, A. Modak³, N. Mohammadi³⁴, A.P. Mohanty⁶³, B. Mohanty⁸⁶, M. Mohisin Khan^{16,v}, Z. Moravcova⁸⁹, C. Mordasini¹⁰⁵, D.A. Moreira De Godoy¹⁴⁴, L.A.P. Moreno⁴⁵, I. Morozov⁶², A. Morsch³⁴, T. Mrnjavac³⁴, V. Muccifora⁵², E. Mudnic³⁵, D. Mühlheim¹⁴⁴, S. Muhuri¹⁴¹, J.D. Mulligan⁸⁰, M.G. Munhoz¹²¹, R.H. Munzer⁶⁸, H. Murakami¹³², S. Murray¹²⁴, L. Musa³⁴, J. Musinsky⁶⁴, C.J. Myers¹²⁵, J.W. Myrcha¹⁴², B. Naik⁴⁹, R. Nair⁸⁵, B.K. Nandi⁴⁹, R. Nania^{10,54}, E. Nappi⁵³, M.U. Naru¹⁴, A.F. Nassirpour⁸¹, C. Natrass¹³⁰, R. Nayak⁴⁹, T.K. Nayak⁸⁶, S. Nazarenko¹⁰⁹, A. Neagu²⁰, R.A. Negrao De Oliveira⁶⁸, L. Nellen⁶⁹, S.V. Nesbo³⁶, G. Neskovic³⁹, D. Nesterov¹¹³, L.T. Neumann¹⁴², B.S. Nielsen⁸⁹, S. Nikolaev⁸⁸, S. Nikulin⁸⁸, V. Nikulin⁹⁸, F. Noferini^{10,54}, P. Nomokonov⁷⁵, J. Norman^{79,127}, N. Novitzky¹³³, P. Nowakowski¹⁴², A. Nyanin⁸⁸, J. Nystrand²¹, M. Ogino⁸², A. Ohlson^{81,104}, J. Oleniacz¹⁴², A.C. Oliveira Da Silva¹³⁰, M.H. Oliver¹⁴⁶, C. Oppedisano⁵⁹, A. Ortiz Velasquez⁶⁹, A. Oskarsson⁸¹, J. Otwinowski¹¹⁸, K. Oyama⁸², Y. Pachmayer¹⁰⁴, V. Pacik⁸⁹, D. Pagano¹⁴⁰, G. Paić⁶⁹, J. Pan¹⁴³, S. Panebianco¹³⁷, P. Pareek^{50,141}, J. Park⁶¹, J.E. Parkkila¹²⁶, S. Parmar¹⁰⁰, S.P. Pathak¹²⁵, B. Paul²³, J. Pazzini¹⁴⁰, H. Pei⁶, T. Peitzmann⁶³, X. Peng⁶, L.G. Pereira⁷⁰, H. Pereira Da Costa¹³⁷, D. Peresunko⁸⁸, G.M. Perez⁸, Y. Pestov⁴, V. Petráček³⁷, M. Petrovici⁴⁸, R.P. Pezzi⁷⁰, S. Piano⁶⁰, M. Pikna¹³, P. Pillot¹¹⁵, O. Pinazza^{34,54}, L. Pinsky¹²⁵, C. Pinto²⁷, S. Pisano^{10,52}, D. Pistone⁵⁶, M. Płoskoń⁸⁰, M. Planinic⁹⁹, F. Pliquet⁶⁸, M.G. Poghosyan⁹⁶, B. Polichtchouk⁹¹, N. Poljak⁹⁹, A. Pop⁴⁸, S. Porteboeuf-Houssais¹³⁴, V. Pozdniakov⁷⁵, S.K. Prasad³, R. Preghenella⁵⁴, F. Prino⁵⁹, C.A. Pruneau¹⁴³, I. Pshenichnov⁶², M. Puccio³⁴, J. Putschke¹⁴³, S. Qiu⁹⁰, L. Quaglia²⁵, R.E. Quishpe¹²⁵, S. Ragoni¹¹¹, S. Raha³, S. Rajput¹⁰¹, J. Rak¹²⁶, A. Rakotozafindrabe¹³⁷, L. Ramello³¹, F. Rami¹³⁶, S.A.R. Ramirez⁴⁵, R. Raniwala¹⁰², S. Raniwala¹⁰², S.S. Räsänen⁴⁴, R. Rath⁵⁰, V. Ratza⁴³, I. Ravasenga⁹⁰, K.F. Read^{96,130}, A.R. Redelbach³⁹, K. Redlich^{85,vi}, A. Rehman²¹, P. Reichelt⁶⁸, F. Reidt³⁴, X. Ren⁶, R. Renfordt⁶⁸, Z. Rescakova³⁸, K. Reygers¹⁰⁴, V. Riabov⁹⁸, T. Richert^{81,89}, M. Richter²⁰, P. Riedler³⁴, W. Riegler³⁴, F. Riggi²⁷, C. Ristea⁶⁷, S.P. Rode⁵⁰, M. Rodríguez Cahuantzi⁴⁵, K. Røed²⁰, R. Rogalev⁹¹, E. Rogochaya⁷⁵,

D. Rohr³⁴, D. Röhrich²¹, P.F. Rojas⁴⁵, P.S. Rokita¹⁴², F. Ronchetti⁵², A. Rosano⁵⁶, E.D. Rosas⁶⁹, K. Roslon¹⁴², A. Rossi^{28,57}, A. Rotondi¹³⁹, A. Roy⁵⁰, P. Roy¹¹⁰, O.V. Rueda⁸¹, R. Rui²⁴, B. Rumyantsev⁷⁵, A. Rustamov⁸⁷, E. Ryabinkin⁸⁸, Y. Ryabov⁹⁸, A. Rybicki¹¹⁸, H. Rytönen¹²⁶, O.A.M. Saari⁴⁴, S. Sadhu¹⁴¹, S. Sadovskiy⁹¹, K. Šafařík³⁷, S.K. Saha¹⁴¹, B. Sahoo⁴⁹, P. Sahoo⁴⁹, R. Sahoo⁵⁰, S. Sahoo⁶⁵, P.K. Sahu⁶⁵, J. Saini¹⁴¹, S. Sakai¹³³, S. Sambyal¹⁰¹, V. Samsonov^{93,98}, D. Sarkar¹⁴³, N. Sarkar¹⁴¹, P. Sarma⁴², V.M. Sarti¹⁰⁵, M.H.P. Sas⁶³, E. Scapparone⁵⁴, J. Schambach¹¹⁹, H.S. Scheid⁶⁸, C. Schiaua⁴⁸, R. Schicker¹⁰⁴, A. Schmah¹⁰⁴, C. Schmidt¹⁰⁷, H.R. Schmidt¹⁰³, M.O. Schmidt¹⁰⁴, M. Schmidt¹⁰³, N.V. Schmidt^{68,96}, A.R. Schmier¹³⁰, J. Schukraft⁸⁹, Y. Schutz¹³⁶, K. Schwarz¹⁰⁷, K. Schweda¹⁰⁷, G. Scioli²⁶, E. Scomparin⁵⁹, J.E. Seger¹⁵, Y. Sekiguchi¹³², D. Sekihata¹³², I. Selyuzhenkov^{93,107}, S. Senyukov¹³⁶, D. Serebryakov⁶², A. Sevcenco⁶⁷, A. Shabanov⁶², A. Shabetai¹¹⁵, R. Shahoyan³⁴, W. Shaikh¹¹⁰, A. Shangaraev⁹¹, A. Sharma¹⁰⁰, A. Sharma¹⁰¹, H. Sharma¹¹⁸, M. Sharma¹⁰¹, N. Sharma¹⁰⁰, S. Sharma¹⁰¹, K. Shigaki⁴⁶, M. Shimomura⁸³, S. Shirinkin⁹², Q. Shou⁴⁰, Y. Sibiriak⁸⁸, S. Siddhanta⁵⁵, T. Siemiarzuk⁸⁵, D. Silvermyr⁸¹, G. Simatovic⁹⁰, G. Simonetti³⁴, B. Singh¹⁰⁵, R. Singh⁸⁶, R. Singh¹⁰¹, R. Singh⁵⁰, V.K. Singh¹⁴¹, V. Singhal¹⁴¹, T. Sinha¹¹⁰, B. Sitar¹³, M. Sitta³¹, T.B. Skaali²⁰, M. Slupecki⁴⁴, N. Smirnov¹⁴⁶, R.J.M. Snellings⁶³, C. Soncco¹¹², J. Song¹²⁵, A. Songmoolnak¹¹⁶, F. Soramel²⁸, S. Sorensen¹³⁰, I. Sputowska¹¹⁸, J. Stachel¹⁰⁴, I. Stan⁶⁷, P.J. Steffanic¹³⁰, E. Stenlund⁸¹, S.F. Stiefelmaier¹⁰⁴, D. Stocco¹¹⁵, M.M. Stortvedt³⁶, L.D. Stritto²⁹, A.A.P. Suaide¹²¹, T. Sugitate⁴⁶, C. Suire⁷⁸, M. Suleymanov¹⁴, M. Suljic³⁴, R. Sultanov⁹², M. Šumbera⁹⁵, V. Šumbera¹⁰¹, S. Sumowidagdo⁵¹, S. Swain⁶⁵, A. Szabo¹³, I. Szarka¹³, U. Tabassam¹⁴, S.F. Taghavi¹⁰⁵, G. Taillepie¹³⁴, J. Takahashi¹²², G.J. Tambave²¹, S. Tang^{6,134}, M. Tarhini¹¹⁵, M.G. Tarzila⁴⁸, A. Tauro³⁴, G. Tejada Muñoz⁴⁵, A. Telesca³⁴, L. Terlizzi²⁵, C. Terrevoli¹²⁵, D. Thakur⁵⁰, S. Thakur¹⁴¹, D. Thomas¹¹⁹, F. Thoresen⁸⁹, R. Tieulent¹³⁵, A. Tikhonov⁶², A.R. Timmins¹²⁵, A. Toia⁶⁸, N. Topilskaya⁶², M. Toppi⁵², F. Torales-Acosta¹⁹, S.R. Torres³⁷, A. Trifiro^{32,56}, S. Tripathy^{50,69}, T. Tripathy⁴⁹, S. Trogolo²⁸, G. Trombetta³³, L. Tropp³⁸, V. Trubnikov², W.H. Trzaska¹²⁶, T.P. Trzcinski¹⁴², B.A. Trzeciak^{37,63}, A. Tumkin¹⁰⁹, R. Turrisi⁵⁷, T.S. Tveter²⁰, K. Ullaland²¹, E.N. Umaka¹²⁵, A. Uras¹³⁵, G.L. Usai²³, M. Vala³⁸, N. Valle¹³⁹, S. Vallero⁵⁹, N. van der Kolk⁶³, L.V.R. van Doremalen⁶³, M. van Leeuwen⁶³, P. Vande Vyvre³⁴, D. Varga¹⁴⁵, Z. Varga¹⁴⁵, M. Varga-Kofarago¹⁴⁵, A. Vargas⁴⁵, M. Vasileiou⁸⁴, A. Vasiliev⁸⁸, O. Vázquez Doce¹⁰⁵, V. Vechernin¹¹³, E. Vercellin²⁵, S. Vergara Limón⁴⁵, L. Vermunt⁶³, R. Vernet⁷, R. Vértesi¹⁴⁵, L. Vickovic³⁵, Z. Vilakazi¹³¹, O. Villalobos Baillie¹¹¹, G. Vino⁵³, A. Vinogradov⁸⁸, T. Virgili²⁹, V. Vislavicius⁸⁹, A. Vodopyanov⁷⁵, B. Volkel³⁴, M.A. Völkl¹⁰³, K. Voloshin⁹², S.A. Voloshin¹⁴³, G. Volpe³³, B. von Haller³⁴, I. Vorobyev¹⁰⁵, D. Voscek¹¹⁷, J. Vrláková³⁸, B. Wagner²¹, M. Weber¹¹⁴, S.G. Weber¹⁴⁴, A. Wegrzynek³⁴, S.C. Wenzel³⁴, J.P. Wessels¹⁴⁴, J. Wiechula⁶⁸, J. Wikne²⁰, G. Wilk⁸⁵, J. Wilkinson^{10,54}, G.A. Willems¹⁴⁴, E. Willsher¹¹¹, B. Windelband¹⁰⁴, M. Winn¹³⁷, W.E. Witt¹³⁰, J.R. Wright¹¹⁹, Y. Wu¹²⁸, R. Xu⁶, S. Yalcin⁷⁷, Y. Yamaguchi⁴⁶, K. Yamakawa⁴⁶, S. Yang²¹, S. Yano¹³⁷, Z. Yin⁶, H. Yokoyama⁶³, I.-K. Yoo¹⁷, J.H. Yoon⁶¹, S. Yuan²¹, A. Yuncu¹⁰⁴, V. Yurchenko², V. Zaccolo²⁴, A. Zaman¹⁴, C. Zampolli³⁴, H.J.C. Zanoli⁶³, N. Zardoshti³⁴, A. Zarochentsev¹¹³, P. Závada⁶⁶, N. Zaviyalov¹⁰⁹, H. Zbroszczyk¹⁴², M. Zhalov⁹⁸, S. Zhang⁴⁰, X. Zhang⁶, Z. Zhang⁶, V. Zherebchevskii¹¹³, D. Zhou⁶, Y. Zhou⁸⁹, Z. Zhou²¹, J. Zhu^{6,107}, Y. Zhu⁶, A. Zichichi^{10,26}, G. Zinovjev², N. Zurlo¹⁴⁰,

Affiliation notes

- ⁱ Deceased
- ⁱⁱ Italian National Agency for New Technologies, Energy and Sustainable Economic Development (ENEA), Bologna, Italy
- ⁱⁱⁱ Dipartimento DET del Politecnico di Torino, Turin, Italy
- ^{iv} M.V. Lomonosov Moscow State University, D.V. Skobeltsyn Institute of Nuclear Physics, Moscow, Russia
- ^v Department of Applied Physics, Aligarh Muslim University, Aligarh, India
- ^{vi} Institute of Theoretical Physics, University of Wrocław, Poland

Collaboration Institutes

- ¹ A.I. Alikhanyan National Science Laboratory (Yerevan Physics Institute) Foundation, Yerevan, Armenia
- ² Bogolyubov Institute for Theoretical Physics, National Academy of Sciences of Ukraine, Kiev, Ukraine
- ³ Bose Institute, Department of Physics and Centre for Astroparticle Physics and Space Science (CAPSS), Kolkata, India
- ⁴ Budker Institute for Nuclear Physics, Novosibirsk, Russia
- ⁵ California Polytechnic State University, San Luis Obispo, California, United States
- ⁶ Central China Normal University, Wuhan, China

- 7 Centre de Calcul de l'IN2P3, Villeurbanne, Lyon, France
- 8 Centro de Aplicaciones Tecnológicas y Desarrollo Nuclear (CEADEN), Havana, Cuba
- 9 Centro de Investigación y de Estudios Avanzados (CINVESTAV), Mexico City and Mérida, Mexico
- 10 Centro Fermi - Museo Storico della Fisica e Centro Studi e Ricerche "Enrico Fermi", Rome, Italy
- 11 Chicago State University, Chicago, Illinois, United States
- 12 China Institute of Atomic Energy, Beijing, China
- 13 Comenius University Bratislava, Faculty of Mathematics, Physics and Informatics, Bratislava, Slovakia
- 14 COMSATS University Islamabad, Islamabad, Pakistan
- 15 Creighton University, Omaha, Nebraska, United States
- 16 Department of Physics, Aligarh Muslim University, Aligarh, India
- 17 Department of Physics, Pusan National University, Pusan, Republic of Korea
- 18 Department of Physics, Sejong University, Seoul, Republic of Korea
- 19 Department of Physics, University of California, Berkeley, California, United States
- 20 Department of Physics, University of Oslo, Oslo, Norway
- 21 Department of Physics and Technology, University of Bergen, Bergen, Norway
- 22 Dipartimento di Fisica dell'Università 'La Sapienza' and Sezione INFN, Rome, Italy
- 23 Dipartimento di Fisica dell'Università and Sezione INFN, Cagliari, Italy
- 24 Dipartimento di Fisica dell'Università and Sezione INFN, Trieste, Italy
- 25 Dipartimento di Fisica dell'Università and Sezione INFN, Turin, Italy
- 26 Dipartimento di Fisica e Astronomia dell'Università and Sezione INFN, Bologna, Italy
- 27 Dipartimento di Fisica e Astronomia dell'Università and Sezione INFN, Catania, Italy
- 28 Dipartimento di Fisica e Astronomia dell'Università and Sezione INFN, Padova, Italy
- 29 Dipartimento di Fisica 'E.R. Caianiello' dell'Università and Gruppo Collegato INFN, Salerno, Italy
- 30 Dipartimento DISAT del Politecnico and Sezione INFN, Turin, Italy
- 31 Dipartimento di Scienze e Innovazione Tecnologica dell'Università del Piemonte Orientale and INFN Sezione di Torino, Alessandria, Italy
- 32 Dipartimento di Scienze MIFT, Università di Messina, Messina, Italy
- 33 Dipartimento Interateneo di Fisica 'M. Merlin' and Sezione INFN, Bari, Italy
- 34 European Organization for Nuclear Research (CERN), Geneva, Switzerland
- 35 Faculty of Electrical Engineering, Mechanical Engineering and Naval Architecture, University of Split, Split, Croatia
- 36 Faculty of Engineering and Science, Western Norway University of Applied Sciences, Bergen, Norway
- 37 Faculty of Nuclear Sciences and Physical Engineering, Czech Technical University in Prague, Prague, Czech Republic
- 38 Faculty of Science, P.J. Šafárik University, Košice, Slovakia
- 39 Frankfurt Institute for Advanced Studies, Johann Wolfgang Goethe-Universität Frankfurt, Frankfurt, Germany
- 40 Fudan University, Shanghai, China
- 41 Gangneung-Wonju National University, Gangneung, Republic of Korea
- 42 Gauhati University, Department of Physics, Guwahati, India
- 43 Helmholtz-Institut für Strahlen- und Kernphysik, Rheinische Friedrich-Wilhelms-Universität Bonn, Bonn, Germany
- 44 Helsinki Institute of Physics (HIP), Helsinki, Finland
- 45 High Energy Physics Group, Universidad Autónoma de Puebla, Puebla, Mexico
- 46 Hiroshima University, Hiroshima, Japan
- 47 Hochschule Worms, Zentrum für Technologietransfer und Telekommunikation (ZTT), Worms, Germany
- 48 Horia Hulubei National Institute of Physics and Nuclear Engineering, Bucharest, Romania
- 49 Indian Institute of Technology Bombay (IIT), Mumbai, India
- 50 Indian Institute of Technology Indore, Indore, India
- 51 Indonesian Institute of Sciences, Jakarta, Indonesia
- 52 INFN, Laboratori Nazionali di Frascati, Frascati, Italy
- 53 INFN, Sezione di Bari, Bari, Italy
- 54 INFN, Sezione di Bologna, Bologna, Italy
- 55 INFN, Sezione di Cagliari, Cagliari, Italy
- 56 INFN, Sezione di Catania, Catania, Italy
- 57 INFN, Sezione di Padova, Padova, Italy

- 58 INFN, Sezione di Roma, Rome, Italy
- 59 INFN, Sezione di Torino, Turin, Italy
- 60 INFN, Sezione di Trieste, Trieste, Italy
- 61 Inha University, Incheon, Republic of Korea
- 62 Institute for Nuclear Research, Academy of Sciences, Moscow, Russia
- 63 Institute for Subatomic Physics, Utrecht University/Nikhef, Utrecht, Netherlands
- 64 Institute of Experimental Physics, Slovak Academy of Sciences, Košice, Slovakia
- 65 Institute of Physics, Homi Bhabha National Institute, Bhubaneswar, India
- 66 Institute of Physics of the Czech Academy of Sciences, Prague, Czech Republic
- 67 Institute of Space Science (ISS), Bucharest, Romania
- 68 Institut für Kernphysik, Johann Wolfgang Goethe-Universität Frankfurt, Frankfurt, Germany
- 69 Instituto de Ciencias Nucleares, Universidad Nacional Autónoma de México, Mexico City, Mexico
- 70 Instituto de Física, Universidade Federal do Rio Grande do Sul (UFRGS), Porto Alegre, Brazil
- 71 Instituto de Física, Universidad Nacional Autónoma de México, Mexico City, Mexico
- 72 iThemba LABS, National Research Foundation, Somerset West, South Africa
- 73 Jeonbuk National University, Jeonju, Republic of Korea
- 74 Johann-Wolfgang-Goethe Universität Frankfurt Institut für Informatik, Fachbereich Informatik und Mathematik, Frankfurt, Germany
- 75 Joint Institute for Nuclear Research (JINR), Dubna, Russia
- 76 Korea Institute of Science and Technology Information, Daejeon, Republic of Korea
- 77 KTO Karatay University, Konya, Turkey
- 78 Laboratoire de Physique des 2 Infinis, Irène Joliot-Curie, Orsay, France
- 79 Laboratoire de Physique Subatomique et de Cosmologie, Université Grenoble-Alpes, CNRS-IN2P3, Grenoble, France
- 80 Lawrence Berkeley National Laboratory, Berkeley, California, United States
- 81 Lund University Department of Physics, Division of Particle Physics, Lund, Sweden
- 82 Nagasaki Institute of Applied Science, Nagasaki, Japan
- 83 Nara Women's University (NWU), Nara, Japan
- 84 National and Kapodistrian University of Athens, School of Science, Department of Physics, Athens, Greece
- 85 National Centre for Nuclear Research, Warsaw, Poland
- 86 National Institute of Science Education and Research, Homi Bhabha National Institute, Jatni, India
- 87 National Nuclear Research Center, Baku, Azerbaijan
- 88 National Research Centre Kurchatov Institute, Moscow, Russia
- 89 Niels Bohr Institute, University of Copenhagen, Copenhagen, Denmark
- 90 Nikhef, National institute for subatomic physics, Amsterdam, Netherlands
- 91 NRC Kurchatov Institute IHEP, Protvino, Russia
- 92 NRC «Kurchatov» Institute - ITEP, Moscow, Russia
- 93 NRNU Moscow Engineering Physics Institute, Moscow, Russia
- 94 Nuclear Physics Group, STFC Daresbury Laboratory, Daresbury, United Kingdom
- 95 Nuclear Physics Institute of the Czech Academy of Sciences, Řež u Prahy, Czech Republic
- 96 Oak Ridge National Laboratory, Oak Ridge, Tennessee, United States
- 97 Ohio State University, Columbus, Ohio, United States
- 98 Petersburg Nuclear Physics Institute, Gatchina, Russia
- 99 Physics department, Faculty of science, University of Zagreb, Zagreb, Croatia
- 100 Physics Department, Panjab University, Chandigarh, India
- 101 Physics Department, University of Jammu, Jammu, India
- 102 Physics Department, University of Rajasthan, Jaipur, India
- 103 Physikalisches Institut, Eberhard-Karls-Universität Tübingen, Tübingen, Germany
- 104 Physikalisches Institut, Ruprecht-Karls-Universität Heidelberg, Heidelberg, Germany
- 105 Physik Department, Technische Universität München, Munich, Germany
- 106 Politecnico di Bari, Bari, Italy
- 107 Research Division and ExtreMe Matter Institute EMMI, GSI Helmholtzzentrum für Schwerionenforschung GmbH, Darmstadt, Germany
- 108 Rudjer Bošković Institute, Zagreb, Croatia
- 109 Russian Federal Nuclear Center (VNIIEF), Sarov, Russia

- 110 Saha Institute of Nuclear Physics, Homi Bhabha National Institute, Kolkata, India
- 111 School of Physics and Astronomy, University of Birmingham, Birmingham, United Kingdom
- 112 Sección Física, Departamento de Ciencias, Pontificia Universidad Católica del Perú, Lima, Peru
- 113 St. Petersburg State University, St. Petersburg, Russia
- 114 Stefan Meyer Institut für Subatomare Physik (SMI), Vienna, Austria
- 115 SUBATECH, IMT Atlantique, Université de Nantes, CNRS-IN2P3, Nantes, France
- 116 Suranaree University of Technology, Nakhon Ratchasima, Thailand
- 117 Technical University of Košice, Košice, Slovakia
- 118 The Henryk Niewodniczanski Institute of Nuclear Physics, Polish Academy of Sciences, Cracow, Poland
- 119 The University of Texas at Austin, Austin, Texas, United States
- 120 Universidad Autónoma de Sinaloa, Culiacán, Mexico
- 121 Universidade de São Paulo (USP), São Paulo, Brazil
- 122 Universidade Estadual de Campinas (UNICAMP), Campinas, Brazil
- 123 Universidade Federal do ABC, Santo Andre, Brazil
- 124 University of Cape Town, Cape Town, South Africa
- 125 University of Houston, Houston, Texas, United States
- 126 University of Jyväskylä, Jyväskylä, Finland
- 127 University of Liverpool, Liverpool, United Kingdom
- 128 University of Science and Technology of China, Hefei, China
- 129 University of South-Eastern Norway, Tonsberg, Norway
- 130 University of Tennessee, Knoxville, Tennessee, United States
- 131 University of the Witwatersrand, Johannesburg, South Africa
- 132 University of Tokyo, Tokyo, Japan
- 133 University of Tsukuba, Tsukuba, Japan
- 134 Université Clermont Auvergne, CNRS/IN2P3, LPC, Clermont-Ferrand, France
- 135 Université de Lyon, Université Lyon 1, CNRS/IN2P3, IPN-Lyon, Villeurbanne, Lyon, France
- 136 Université de Strasbourg, CNRS, IPHC UMR 7178, F-67000 Strasbourg, France, Strasbourg, France
- 137 Université Paris-Saclay Centre d'Etudes de Saclay (CEA), IRFU, Département de Physique Nucléaire (DPhN), Saclay, France
- 138 Università degli Studi di Foggia, Foggia, Italy
- 139 Università degli Studi di Pavia, Pavia, Italy
- 140 Università di Brescia, Brescia, Italy
- 141 Variable Energy Cyclotron Centre, Homi Bhabha National Institute, Kolkata, India
- 142 Warsaw University of Technology, Warsaw, Poland
- 143 Wayne State University, Detroit, Michigan, United States
- 144 Westfälische Wilhelms-Universität Münster, Institut für Kernphysik, Münster, Germany
- 145 Wigner Research Centre for Physics, Budapest, Hungary
- 146 Yale University, New Haven, Connecticut, United States
- 147 Yonsei University, Seoul, Republic of Korea